CHARACTERIZING SYNOPTIC AND CLOUD VARIABILITY IN THE NORTHERN ATLANTIC USING SELF-ORGANIZING MAPS

BY

Carly Fish

Submitted to the graduate degree program in Geography and the Graduate Faculty of the University of Kansas in partial fulfillment of the requirements for the degree of Master of Science

---

Dr. David Mechem
Chairperson

Nathaniel Brunsell

David Rahn

Date Defended: July 8, 2014

The Thesis Committee for Carly Fish
certifies that this is the approved version of the following thesis:

CHARACTERIZING SYNOPTIC AND CLOUD VARIABILITY IN THE

NORTHERN ATLANTIC USING SELF-ORGANIZING MAPS

Dr. David Mechem
Chairperson

Date Approved: July 8, 2014

ABSTRACT

CHARACTERIZING SYNOPTIC AND CLOUD VARIABILITY IN THE NORTHERN ATLANTIC USING SELF-ORGANIZING MAPS

Carly Fish

Department of Geography

Master of Science

Low-level clouds have a significant influence on the Earth's radiation budget and it is thus imperative to understand their behavior within the marine boundary layer (MBL). The cloud properties in the Northeast Atlantic region are highly variable in space and time and are a research focus for many atmospheric scientists. Characterizing the synoptic patterns in the region through the implementation of self-organizing maps (SOMs) enables a climatological grasp of cloud and atmospheric fields. ERA–Interim and MODIS provide the platform to explore the variability in the Northeast Atlantic for over 30 years of data. Station data comes from CAP–MBL on Graciosa island in the Azores, which lies in a strong gradient of cloud and other atmospheric fields, offer an opportunity to incorporate an observations for the years of 2009 and 2010.

ACKNOWLEDGMENTS

I would like to thank my advisor, Dr. David Mechem for the wonderful opportunity to be his Graduate Research Assistant and for all of his patient assistance through my research. I would also like to thank Nathaniel Brunsell and David Rahn for taking the time to serve on my thesis committee and for their valuable insights throughout my graduate studies. Thank you to Sandra Yuter, Matthew Miller and Simon de Szoeke for their collaboration on this research. Thank you to Adriana Bailey at the University of Colorado who brought the SOM classification method to our attention and to Aaron Kennedy for thoughtful insight through the SOM classification process. Thank you to the Department of Energy for providing the funding to make this all possible. Thank you to Shu Chen for his initial guidance with the SOM algorithm. Thank you to CISL, ASR, and MODIS for data platforms used within this study. Finally, I would like to thank my parents, Gary and Melinda Fish, for encouraging me though out my education.

Contents

List of Figures

List of Tables

Chapter 1

Introduction

Global climate models (GCMs) are host to many uncertainties, with some of the greatest issues stemming from misrepresented low-level clouds (Bony and Dufresne, 2005; Medeiros et al., 2008). Stratocumulus in particular cover more of the Earth's surface than any other type of cloud and play an important role in the Earth's radiation budget (Hartmann et al., 1992; Warren et al., 1986). Stratocumulus are commonly associated with the descending branches of the Hadley and Walker circulations (Schubert, 1976) and are most frequently found over oceans (Klein and Hartmann, 1993). Stratocumulus clouds persist in the eastern portions of ocean basins, in the presence of cool upwelling ocean waters (Paluch and Lenschow, 1991). Though they are often perceived as horizontally homogeneous, stratocumulus clouds are highly variable in space and time (Klein, 1997; Klein et al., 1995).

The Northeast and Southeast Pacific (NEP and SEP, respectively) regions are well known for large sheets of stratocumulus clouds and have been common places for field campaigns to study low-level cloud properties and dynamics. Findings from field campaigns such as FIRE (First ISCCP Regional Experiment; Albrecht et al. 1988) and DYCOMS–II (Dynamics and Chemistry of Marine Stratocumulus; Stevens et al. 2003)

in the NEP, and EPIC (Eastern Pacific Investigation of Climate; Bretherton et al. 2004) and VOCALS–REx (VAMOS Ocean-Cloud Atmospheric-Land Study Regional Experiment; Wood et al. 2011) in the SEP, have contributed to the understanding of turbulence, precipitation, vertical structure, entrainment, chemical composition, evolution, lifecycle, and radiative properties within stratocumulus.

The progression of the stratocumulus-to-cumulus was the focus of the ASTEX (Atlantic Stratocumulus Transition Experiment) field campaign, which took place in 1992 in the eastern North Atlantic region (Albrecht et al., 1995). ASTEX emphasized the transition of a shallow, well-mixed marine boundary layer (MBL) to a deeper, decoupled MBL with distinct subcloud and cloud-layer circulations. When low-level clouds were advected over warmer sea surface temperatures (SSTs), cloud fraction was observed to decrease as the deepening MBL was accompanied by the breakup of stratocumulus into cumulus (Albrecht et al., 1995). ASTEX observations highlighted the roles that solar absorption, drizzle, and deepening play in decoupling of the MBL.

The findings from ASTEX in union with the Pacific field campaign studies motivated the 21-month deployment of the Aerosol Radiation Measurement (ARM) Mobile Facility (AMF) on Graciosa Island in the Azores (Wood et al., 2014). The goal of the Clouds, Aerosol, and Precipitation in the Marine Boundary Layer (CAP–MBL) field campaign was to study the processes that control the radiative and microphysical properties in MBL clouds. The Azores were chosen because of their ideal location to sample the climatological transition from overcast stratocumulus in the springtime to broken trade cumulus in the summer. Observations from CAP–MBL show that low-level clouds are present between 40 and 60% of the time, with a maximum in summer and fall, which negatively correlates with the maximums of all other cloud types (Rémillard et al., 2012). They also found that high clouds are a primary driver of the seasonal cycle of overall cloudiness (Rémillard et al., 2012). The substantial amount

of variability during the 21-month deployment generated traction for the Azores to become a permanent ARM site starting in October 2013 (Wood et al., 2014).

The environment in the vicinity of the Azores is substantially influenced by the synoptic-scale structure, which strongly governs the thickness and coverage of stratocumulus (Wood, 2012). Stratocumulus are frequently found just east of a midtropospheric ridge axis, where the presence of a subtropical high is associated with large-scale subsidence (Norris, 1998; Norris and Klein, 2000). This subtropical high, or Bermuda High, is present in nearly all flow regimes in the summertime (Li et al., 2011). The strength (magnitude of the central high pressure) of this Bermuda High varies, and its interaction with the Icelandic Low can also impact the large-scale flow that influences the prime locations for stratocumulus. The dynamics of the interactions between the Bermuda High and Icelandic Low over the Northeast Atlantic (NEA) are quantified by the North Atlantic Oscillation (NAO) index, which can be used to characterize common climatological patterns. These teleconnection patterns have an influence on storm tracks, which also impact MBL structure and stratocumulus location (Folland et al., 2009).

Though influences like the storm track modulate the location of stratocumulus, the primary requirement for their formation is the prevalence of a strong temperature inversion, promoting the accumulation of low-level moisture (Paluch and Lenschow, 1991). If sufficiently strong, this inversion can discourage the mixing of drier air from above the cloud layer, which would otherwise lead to evaporative cooling, negative buoyancy, and ultimately, the disintegration of the cloud layer (Lilly, 1968). The strength of the inversion is partially reflected in the lower-tropospheric stability, which has been found to be highly important for the presence of low-level clouds (Klein and Hartmann 1993, KH93 hereafter). However, preliminary analysis of the CAP–MBL period suggests that the relationship between stability and cloud fraction may not

be as robust as previously established, at least on short timescales (S. de Szoeke, personal communication).

The relationship between the general circulation and stratocumulus regimes is well established, but much uncertainty exists about the regional dependence of stratocumulus cloud properties on the synoptic state, and more importantly, the influence of synoptic state on these cloud properties. The technique of synoptic classification provides a means to characterize a variety of synoptic states in the NEA. The established classes, or synoptic states, will be used to examine the relationships between the environmental characteristics of each synoptic state and its accompanying cloud properties, thus exploring stratocumulus variability on a regional scale.

Synoptic classification techniques have evolved through a wide range of purposes and approaches, each with inherent assumptions and advantages, but all with the overarching goal of establishing synoptic-scale circulations and their relation to local or environmental responses (Hewitson and Crane, 2002). Though the concept of synoptic classification can be pinpointed as far back as the late 19th century (Abercromby 1883; Köppen 1874), it became a distinguished field within climatology after the publication of 'Synoptic Climatology: Methods and Applications' by Barry and Perry (1973). They describe the purpose of synoptic climatology as gaining insight into local or regional climates through exploring the relationship of weather elements to large-scale atmospheric circulation.

Synoptic classification has most commonly been used as a data reduction technique for large data sets (Crane, 1978), but has also been used to extend local data records back in time through the use of a transfer function with frequently experienced synoptic states (Barry and Perry, 1973). Synoptic classification approaches have been described through variety of techniques, the oldest of which is synoptic typing. Synoptic typing has a longer history due its more simplistic two stage

approach of first, the classification of broad atmospheric circulation patterns, and second, determining the relationships between the circulation patterns with the local surface environment (Yarnal and Draves, 1993). Synoptic typing can be further categorized by a circulation-to-environment or environment-to-circulation approach, and are employed depending on the scientific question of the study. Environment-to-circulation uses local variables to classify the large-scale circulation patterns, while circulation-to-environment starts with the large-scale circulation to describe the local environment.

The early methods for synoptic classification, and more specifically synoptic typing, were done manually. Lamb (1950) classified over 18,000 records into seven synoptic types by hand based on the position of low and high-pressure systems relative to the British Isles (Lamb, 1950). Though this method was effective, it was incredibly labor intensive. A vast number of automated approaches have been developed to alleviate this labor-intensive nature of synoptic typing. Examples of popular algorithms include k-means clustering and eigenfunction analysis. One study used an environment-to-circulation based approach, applying the k-means classification over ISCCP (International Satellite Cloud Climatology Project) cloud data products to generate weather states for the globe (Tselioudis et al., 2013). They have since compared the weather states at the Azores with their global weather states, and found that the Azores experience similar weather states to the rest of the globe, but do experience low-cloud weather states more frequently (Wood et al., 2014). This approach generated the weather states associated with certain cloud regimes for roughly a two-year period, but a circulation-to-environment approach would also be of value to examine the typical circulation patterns and associated cloud regimes around the Azores, especially over a climatological time-scale. This synoptic typing would provide a climatological background for the typical meteorological conditions experienced

at and around the Azores. A climatological background in this region would be useful to interpret past, present, and future ARM data findings.

Synoptic typing has trade-offs, however, primarily concerning a large degree of within-group variability. There may also be issues with a variety of environmental responses associated with the days within a synoptic state, or that an environmental response can be obtained from multiple synoptic states. These approaches generate a first-order understanding of a particular synoptic classification, but overgeneralization may limit the ability to capture the full range of synoptic variability within the dataset.

These trade-offs provide incentive for more mathematically intensive forms of synoptic classification. Such approaches are typically automated, providing ease for the researcher. Common approaches include principal component analysis (PCA) and artificial neural nets (ANN). ANNs are an attractive approach because of the way it treats the data as a continuum, allowing for relationships between the synoptic states. A potential disadvantage of some of the mathematically rigorous techniques, however, is the loss of interpretability and physical significance of synoptic states.

Some sort of mathematical-based approach that retains the interpretability associated with synoptic typing would be advantageous to develop a synoptic climatology for the NEA region. This would require an approach that would treat the data as a continuum while preserving interpretability of the subsequent weather states. One clustering method that has developed attention in the atmospheric science community is the technique of self-organizing maps (SOMs, Kohonen 1990). SOMs are a type of ANN, but apply a neighborhood function that preserves the topology of the SOM (explained further in the Methodology). SOMs are similar to other traditional forms of cluster analysis, such as k-means clustering, where nodes are distributed within a cloud of data, assigning more nodes in regions of higher densities of data.

There are two main differences between SOMs and other forms of cluster analysis. The first difference lies in the primary goal of the SOM when establishing nodes, which is to create a continuum of nodes that cumulatively represent the multi-dimensional distribution of the entire data set, rather than simply representing individual clusters of data. When a data sample is matched to a node (described in detail in the Methodology), the surrounding nodes are updated in addition to the matching node, which distinguishes the SOM clustering approach from k-means clustering. The second main difference is the interpretability of the resulting SOM nodes. PCA generates patterns that have forced orthogonally and may lose physical significance for some components, whereas SOM nodes depict synoptic patterns.

Hewitson and Crane introduced SOMs into physical geography in 1994 to generate a general discussion of neural networks within the community (Hewitson and Crane, 1994). Examples include Cavazos (2000) who used SOMs as a method for climate classification, Ambroise et al. (2000) who experimented with the SOM approach on cloud classification, and Cassano et al. (2006) used SOMs to generate nodes to predict extreme weather events for the remote regions of Barrow, Alaska.

We employ the technique of SOMs to characterize synoptic states over the North Atlantic region and to explore the joint variability of atmospheric and cloud properties in the vicinity of the Azores. The primary objective of this study is to contribute to the general understanding of the behavior of low-level clouds and to explore the joint variability in synoptic configuration and low-cloud properties over the NEA by pursuing the following questions:

(1) Through the implementation of self-organizing maps, what are the dominant synoptic states over the North Atlantic Ocean?

(2) What are the characteristics of cloud properties associated with these dominant synoptic states?

To address the first question, the self-organizing map algorithm is applied to the 500-mb geopotential height field, where the identification of troughs, ridges, and transitional flow regimes provides insight to the atmospheric behavior in the Northern Atlantic. The second question aims to find links between stratocumulus cloud properties and the synoptic-scale configuration over the NEA. The following are testable hypotheses to be evaluated:

1a. Summer synoptic states are dominated by the Bermuda High, but states with a less intensive high permit synoptic intrusions from higher latitudes.

1b. Winter synoptic states are associated with a greater variety of flow patterns, which are strongly tied to characteristics of the Icelandic Low.

2a. Following the findings from Norris and Klein (2000, Part III), areas associated with low-level divergence, subsidence and a surface ridge will support ordinary stratocumulus.

2b. Calculating joint probability density functions (PDFs) for each synoptic state will reveal a better relationship between cloud properties and synoptic factors than calculating joint PDFs for the entire monthly data sets alone.

Chapter 2

Data

A diverse suite of data types are used in this study to explore stratocumulus variability over the Northern Atlantic. The SOM calculations are based on ERA–Interim reanalysis (Dee, 2011) from the CISL Research Data Archive (managed by NCEP with data from ERA–Interim products, http://rda.ucar.edu/). The analysis spans January 1979 to October 2012 with data output every six hours. Geopotential heights and vertical velocity were obtained at 1000-mb, 850-mb, 700-mb and 500-mb pressure levels, while cloud fraction (CF), temperature, mixing ratio, and liquid and ice condensate were obtained for all available pressure levels. The SOM analysis employed data at 0000 UTC to avoid diurnal variations. The data used are summarized in Table 2.1.

Bulk cloud fraction (calculated from all available vertical levels), as well as low (1000-700mb), medium (700-450mb) and high (450-50mb) levels are calculated as closely as possible to the ISCCP (International Satellite Cloud Climatology Project) cloud definitions (Rossow and Schiffer, 1999).

The area covered by the reanalysis data domain included the heart of the Northern Atlantic Ocean, between approximately 25° to 55°N and 50° to 10°W, as seen in the smaller, outlined domain in Figure 2.1. The data are on a regularly spaced

Table 2.1 Data sources used for study.

ERA–Interim	CAP-MBL	MODIS
geopotential height	temperature	total cloud fraction
vertical velocity	water vapor mixing ratio	liquid cloud fraction
cloud fraction	liquid water path	ice cloud fraction
temperature		mixed cloud fraction
mixing ratio		unknown cloud fraction
liquid/ice water content		cloud top temperature
sea surface temperature		
surface pressure		

latitude–longitude grid ($0.7^\circ \times 0.7^\circ$ grid spacing), resulting in an analysis domain of 42 points (latitude) by 57 points (longitude). The synoptic fields for this domain are to assess the dominant synoptic states over the NEA.

In addition to the ERA–Interim products, the analysis employed observational data from the CAP–MBL deployment of the Department of Energy (DOE) ARM Mobile Facility (AMF) from May 2009 through December 2010 on Graciosa Island ($39^\circ\ 5'\ 28''$N, $28^\circ\ 1'\ 45''$W,15.24m.), which is a small island in the Azores Island chain. The Azores experience both relatively clean marine air masses and more polluted continental air masses from North America and European origins.

MODIS (Moderate Resolution Imaging Spectroradiometer) retrievals of cloud fraction from Dr. Matthew Miller at North Carolina State University add an essential satellite element to the study. The MODIS data came from the Aqua (1:30 am and pm, local time over pass) satellite (Platnick et al., 2003). These data span the period from 2002 to 2012, and were used in union with the reanalysis. The MODIS cloud retrievals constitute observations of clouds over the NEA, in addition to using

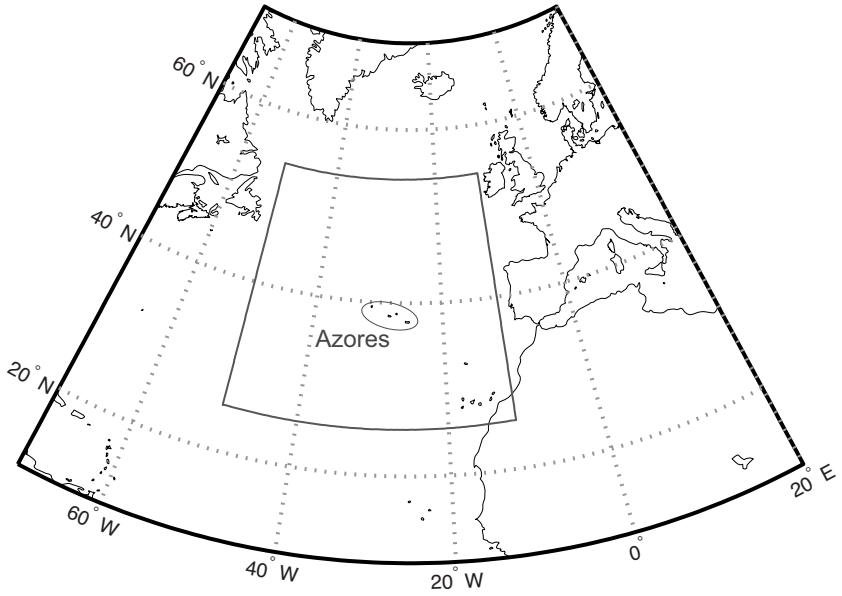

Figure 2.1 The North Atlantic region around the Azores, with the small outlined domain used for the SOM.

ERA–Interim cloud fields to study the characteristic cloud properties for the dominant synoptic states. MODIS products offer total, liquid, mixed-phase, and ice-phase cloud fraction retrievals. MODIS cloud fraction properties come from MYD06_L2 SDS and MODIS products are stored on a 1 degree by 1 degree equal area grid. Comparing MODIS cloud properties directly to cloud fraction from reanalysis, however, is not trivial, largely because of the possible occurrence of overlapped clouds. The presence of high cloud will mask low cloud and cause a systematic underestimate in low/liquid cloud fraction. To sidestep some of these difficulties, we restrict our analysis to total cloud fraction and cloud top temperature (CTT), which we take as a measure of the highest cloud layer. This CTT is aggregated into day and night quantities from the MYD06_L2 SDS Cloud_Mask_5km MODIS product. A summary of the data products used from the different sources are presented in Table 2.1.

Chapter 3

Methodology

A synoptic classification of the highly variable Northern Atlantic region requires a technique that is capable of representing the wide range of atmospheric and cloud properties. We employ the technique of self-organizing maps to classify synoptic state. SOMs were introduced by Kohonen in 1981 and have a wide range of applications such as speech recognition, optimization problems, and insect classification (Kohonen, 1990). Hewitson and Crane (2002) described in detail the application of SOMs to synoptic climatology and how SOMs offer "a mechanism for visualizing the complex distribution of synoptic states, yet [treat] the data as a continuum."

3.1 Self-organizing maps

Following the approach of Hewitson and Crane (2002), we used the SOM technique to find characteristic synoptic states. Each SOM node is associated with a set of dates that are uniquely mapped to one node. A record for the dates associated with each node will be cumulatively referenced to as the SOM "codebook." The distribution of the user-defined number of nodes is dependent on the distribution of the

data, allowing more nodes to represent synoptically similar input data. Competitive learning directs the input data to its best matching (or winning) node. As the competitive learning process takes place, nodes surrounding the winning node (or neighborhood nodes), adjust toward the winner. The competitive learning stage also employs a neighborhood function to update not only the winning node, but the surrounding nodes as well. This neighborhood function is what distinguishes the SOMs from a k-means clustering approach. The competitive learning and adjustment of the nodes happens independently of the user, and thus the SOM analysis constitutes an unsupervised learning process, ultimately resulting in an objective classification of synoptic states.

Like other clustering algorithms, SOMs maximize between-group differences while minimizing within group differences (Bailey et al., 2011). The SOM analysis results in a web of synoptic states representing the input data as a continuum, rather than independent synoptic types, where the SOM nodes display persistent and transitional states. Unlike the eigenmodes in empirical orthogonal functions (EOFs), SOM analysis does not enforce orthogonality among the nodes, and aspects of non-linearity within input data will be represented. This non-orthogonality makes the SOM procedure fundamentally different from linear approaches.

Using a toolbox written in MATLAB (www.cis.hut.fi/projects/somtoolbox), monthly SOMs are created and used to further explore the Northern Atlantic synoptic states. The SOM analysis of synoptic states is based on the 500-mb geopotential height field, largely because of its importance in governing the large-scale meteorological forcing and the relatively smooth nature of the field. Though some studies use 1000-mb geopotential heights to initialize the SOM, we selected 500-mb because of the overwhelming dominance of the Bermuda High at the surface level. Normalized anomalies are calculated from this field to ensure a study of meteorological variability, instead of

latitudinal variations. This is calculated by subtracting a 31-day centered mean (±15 days) from each data sample, and then dividing that day by the standard deviation of that 31-day window. Finally, an equal area assumption is applied (cos(latitude)), which is used to avoid heavier weights in the polar regions (Gong and Wang, 1999). The calculation to generate the normalized anomalies of 500-mb geopotential heights, $\langle Z \rangle$, is shown in Equation 3.1. The SOM is applied to normalized anomalies for 500-mb geopotential heights at 0000 UTC for each month which results in 12 individual codebooks, each containing the same number of synoptic states.

$$\langle Z \rangle = \frac{\left(Z - \bar{Z}\right)}{\sigma_Z} \cos \phi \tag{3.1}$$

In order to represent the full continuum of synoptic behavior for over 30 years of data, it is imperative to choose a large enough number of SOM nodes. Too few nodes overgeneralize the data and potentially combine distinct states into too few categories; however, too many nodes create an overwhelming number of synoptic states to decipher, with similar synoptic states spread across multiple nodes. Since the number of SOM nodes is user-defined, we had to approach the map-size with caution. One way to identify an optimal number of nodes is to run the SOM algorithm across a range of different map sizes (2×2 to 10×10) and evaluate different error metrics. We evaluated the inherent error for these maps (both quantization and topographic) to assist us in choosing the optimal map-size.

Following the concept of the elbow criterion (Tibshirani et al., 2001), the quantization error (the average euclidian distance between the data and its best matching unit, or BMU) for a range of map sizes is evaluated, which decreases with increasing number of nodes. The elbow criterion describes the point at which the addition of nodes 'fail to add a significant amount of information' (Schuenemann et al., 2009) to the SOM, justifying the lower bound for number of nodes absolutely necessary to

represent the input data. The topographic error (the measure of how much of the input data have non adjacent BMUs and secondary BMUs) exhibits behavior opposite to the quantization error. The topographic error increases as the number of nodes increases because the codebook becomes more complex as successive data are more likely to be mapped to nonadjacent nodes. The point at which adding nodes drastically increases the topographic error created an upper bound for the ideal codebook size. Tests using the July ERA–Interim reanalysis suggests that a map of 25 nodes (5 $\times$ 5) is the optimal size to use for this study (the elbow plot used is in the Appendix).

3.2 Statistical significance

The absolute and relative frequency of each node will be explored to assess the tendency for data to favor individual nodes relative to each month. Statistical significance of individual nodes is described using a 95% confidence interval (Schuenemann et al., 2009):

$$p \pm 1.96 \left(\frac{p(1-p)}{n} \right)^{\frac{1}{2}} \tag{3.2}$$

The probability (p) of a record being mapped to a node is 1/N, where N is the number of nodes (25) chosen for the SOM. A 95% confidence level for the data is therefore calculated by where n is the number of input records for the SOM. If the frequency of a node falls outside of this confidence interval, it will be considered statistically significantly high (or significantly low). For example, the expected frequency for each node for a 5 $\times$ 5 codebook is 4.0% (1/25). A dataset with 1054 records, for instance, would then have a 95% confidence interval of 2.82%-5.18%, with frequency values outside of that range deemed statistically significant. The significantly high nodes will demand attention because of their high rate of relevance, but significantly

low nodes may offer value as an avenue of transition between higher frequency nodes.

Transitions between the nodes are also evaluated, revealing the tendencies for input data to be mapped near each other (not shown). These forward (backward) trajectories therefore represent the evolution of one synoptic state to another (from another), or a tendency to remain at the same state, suggesting persistence of a synoptic pattern. Individual node errors will also be calculated from the mean of the error of each input data to its BMU, showing which nodes are more representative of their input data, and which nodes contain more intra-node discrepancies.

3.3 Projections of environmental and cloud properties

The SOM codebook of dates was used to project the corresponding atmospheric and cloud properties onto each node, by compositing the mean environmental or cloud pattern for each node. The projections of atmospheric variables onto the SOM nodes thus allow for further understanding of the spatial distribution for each node. It is important to note that these projected variables have no influence on the SOM analysis, which employs only the normalized 500-mb geopotential height anomaly field. The projected variables included in this study are the 1000-mb geopotential heights, ERA–Interim and MODIS total cloud fraction and cloud top temperature (CTT), total condensate (the sum of liquid and ice water contents), stability (estimated inversion strength, EIS), and vertical velocity.

Total cloud cover is generated from ERA–Interim cloud fraction at the reanalysis pressure levels, using a maximum-random overlap assumption (C_{maxran}, Morcrette and Fouquart (1986); Oreopoulos and Khairoutdinov (2003)). This maximum-random overlap assumption assumes that adjacent layers are overlapped maximally, while

nonadjacent blocks are overlapped randomly. The equation is given in Equation 3.3 below, where C_1 represents the first cloud layer, and C_i and C_{i-1} represent adjacent cloud layers.

$$C_{maxran} = 1 - (1 - C_1) \times \prod_{i=2}^{N} \frac{1 - \max(C_{i-1}, C_i)}{1 - C_{i-1}} \tag{3.3}$$

Cloud top temperature is calculated using the highest point at which cloud is present, using liquid and ice content thresholds. Given the discrete nature of the pressure levels in the data set, the actual highest point of cloud may be underestimated somewhat, thus, CTT may be overestimated (too warm). The CTT calculation was not particularly sensitive to threshold values.

Temperature and water vapor mixing ratio from reanalysis is used to quantify lower-atmosphere stability. The most straightforward way to quantify stability of the MBL is lower tropospheric stability (LTS). LTS is defined as the difference between the potential temperature at 700mb and the surface (Klein and Hartmann, 1993).

$$LTS = \theta_{700} - \theta_{surface} \tag{3.4}$$

A more reliable predictor than LTS in quantifying the strength of the inversion is estimated inversion strength (EIS), which is based on LTS but subtracts out the moist static stability, as seen in Equation 3.5 below (Wood and Bretherton, 2006).

$$EIS = (\theta_{700} - \theta_{surface}) - \Gamma_m^{850}(z_{700} - LCL) \tag{3.5}$$

Projections of MODIS and ERA–Interim cloud fraction onto the SOM nodes illustrate the mean spatial distribution of cloud cover for each node. Since MODIS does not have an equivalent ISCCP low-level cloud product, CTT is used for both ERA–Interim and MODIS because of its implications for this vertical distribution of

cloud properties. Though nighttime Terra retrievals (10:30 pm) are closer in time to the 0000 UTC ERA–Interim data used, night Aqua retrievals (1:30 am) are used because of a persistent, cone-shaped artifact in the Terra cloud fraction products. Projecting total condensate offers another measure of cloud properties in addition cloud fraction and CTT. Joint variability between cloud fraction and different forcing fields (vertical velocity and EIS) will also be examined.

Chapter 4

Results

Running the SOM algorithm first with the 25 node map size on the entire data set of normalized 500-mb anomalies and then parsing the nodes into archetypal synoptic states reveals extremely different synoptic signatures for winter and summer months, as seen in Figure 4.1. Ridge, trough, pre-trough, post-trough and zonal categories are used to characterize the states, starting with the master normalized 500-mb anomaly SOM map. Anomoulously high normalized geopotential heights are considered ridge-like, while anomolously low geopotential heights are trough-like, given a SOM with a nearly zero middle (climatological mean) pattern. Nodes with negative (positive) anomalies intruding into positive (negative) anomalies are pre-trough (post-trough). Nodes that are laterally homogeneous with positive anomalies are considered zonal, and everything else falls under unclassified. For boundaries between patterns, 500-mb projected heights were also considered for extra guidance for optimal characterization. Summer is characterized by its ridge and zonal like patterns, while winter is predominately trough and post-trough type patterns. June, September and October have the highest accounts of pre-trough states. The actual values are given in Table 4.1.

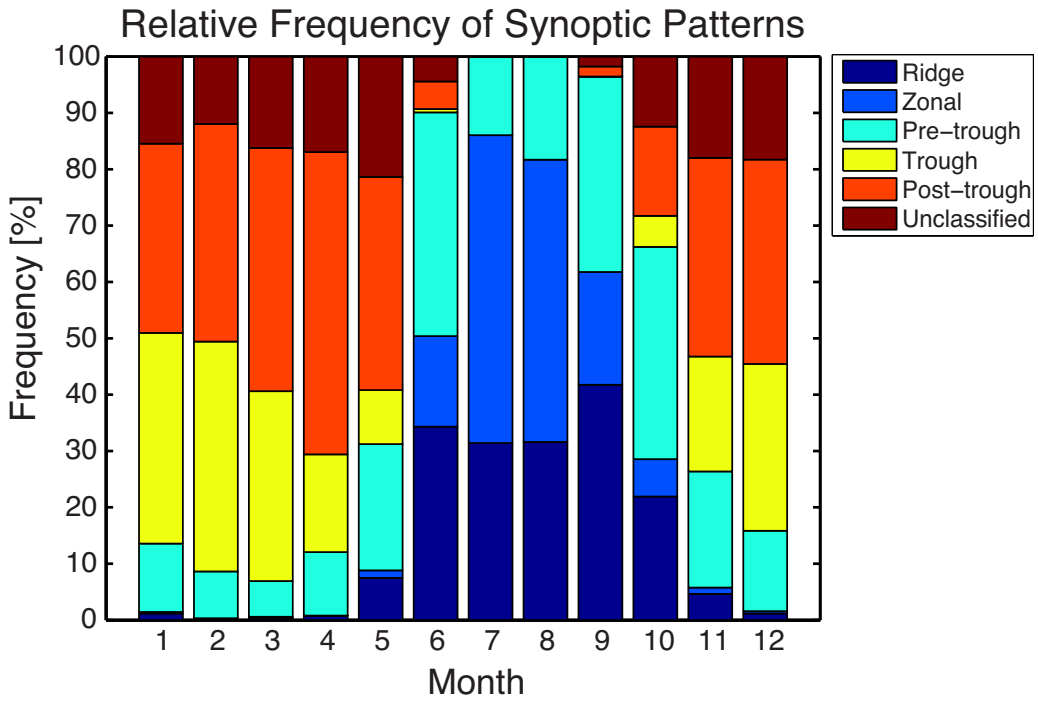

Figure 4.1 Annual cycle of ridge, zonal, pre-trough, trough, post-trough and unclassified patterns for the annual SOM nodes.

According to this annual perspective of the data set, summer months never see synoptic intrusions associated with a trough pattern, and the winter months are generally dominated by trough and post-trough weather patterns, without any ridge features. This necessitates a closer examination on a month to month scale, running the SOM algorithm on all months individually. This should provide further explanation into this potentially misleading figure of winter and summer months.

Table 4.2 shows the frequency of occurrence that each month experiences ridges, troughs, pre-troughs, post-troughs, zonal and unclassified patterns, as determined from the 12 individual monthly SOMs. This shows that there is a greater variety of flow patterns experienced within each month. January experiences ridge like conditions 25.4% of the time, with is much greater (and more realistic) than what is shown from the annual SOM patterns. June experiences synoptic intrusions 20.5% of the

Table 4.1 Percentages of synoptic patterns experienced during each month.

	Pre-trough	**Trough**	**Post-trough**	**Ridge**	**Zonal**	**Unclassified**
January	12.1	37.4	33.6	1.1	0.3	15.5
February	8.3	40.8	38.6	0.3	0.0	12.0
March	6.4	33.7	43.2	0.4	0.2	16.2
April	11.3	17.4	53.6	0.8	0.0	17.0
May	22.4	9.6	37.9	7.5	1.3	21.3
June	39.7	0.6	4.9	34.3	16.1	4.4
July	13.9	0.0	0.0	31.4	54.6	0.0
August	18.3	0.0	0.0	31.6	50.1	0.0
September	34.7	0.0	1.8	41.8	20.0	1.8
October	37.7	5.5	15.8	21.9	6.6	12.4
November	20.6	20.4	35.3	4.6	1.1	18.0
December	14.3	29.6	36.3	1.2	0.4	18.3

time, which is greater than what might be expected given the dominant Bermuda High in the summertime months.

The annual cycle for ERA–Interim total and low-level cloud fraction and MODIS total cloud fraction for Graciosa is seen in Figure 4.2. Error bars for ERA –Interim are included for total and low cloud fraction. The cycle for ERA –Interim and MODIS total cloud fraction are largely the same, although MODIS is consistently greater. Error bars show great variability in total and low cloud fraction within each month for Graciosa, The maximum total cloud fraction is in the wintertime months, with a minimum in the late summer and early fall, which is consistent with the 21-month AMF results (Figure 3 from Rémillard et al. 2012). Low-level clouds have a maximum in June, followed by a minimum in the late summer and early fall.

June is the month of highest low-level cloud amount (Figure 4.2 and Figure 3b

Table 4.2 Percentages of synoptic patterns experienced during each month from the 12 monthly codebooks.

	Pre-trough	**Trough**	**Post-trough**	**Ridge**	**Zonal**	**Unclassified**
January	21.1	17.2	8.4	25.4	17.1	10.8
February	10.9	21.6	18.4	26.5	15.6	7.1
March	14.5	21.8	18.0	34.6	0.0	11.1
April	24.0	13.9	20.6	24.7	13.1	3.6
May	17.7	30.0	24.5	21.3	6.6	0.0
June	22.6	20.5	25.1	21.7	9.8	0.0
July	0.0	30.3	38.6	16.8	14	0.0
August	8.2	22.6	26.5	26.1	9.2	7.3
September	11.6	26.0	18.2	20.3	19.9	3.6
October	23.6	17.7	33.1	18.1	2.8	4.5
November	21.2	14.9	24.6	30.6	3.7	5.1
December	11.7	26.4	10.0	27.9	12.2	11.6

from Rémillard et al. 2012). The annual cloud cover maximum occurs during winter, with also includes substantial low cloud coverage. January is representative of this cloud cover maximum and typical winter conditions. Figure 4.3 shows the mean 500-mb height structure for January and June. January exhibits greater variability in the 500-mb height field, and thus greater storm track variability. Areas of low pressure in the northwest portion of the domain are associated with the presence of the Icelandic low in wintertime months. June has less variation in 500-mb heights in the north-south direction, and has a large area of high heights around 20°N, indicative of the presence of the Bermuda High. This Bermuda High modulates the region, which accounts for the lower values of storm track variability at lower latitudes.

Although we run the SOM algorithm on each month, we chose to highlight January

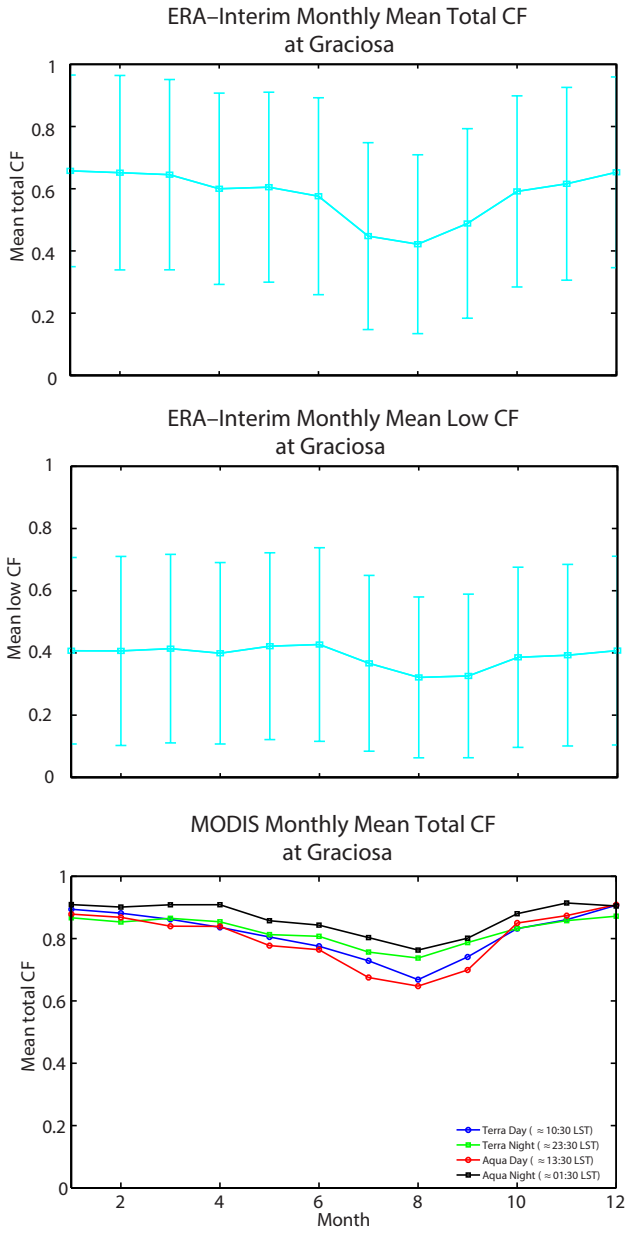

Figure 4.2 Annual amounts of low and total cloud fraction with respective error bars. Total cloud cover suggests that January is a reasonable representation for the maximum total cloud coverage during wintertime months. Low-level clouds show that June has the maximum low-level cloud coverage and August and September have minimum low-level cloud coverage, showing a substantial drop-off in low-level cloud coverage from summer to fall months.

and June because of their significance to the annual cloud cycle. For the SOM nodes and projected quantities for the rest of the months, please contact the author.

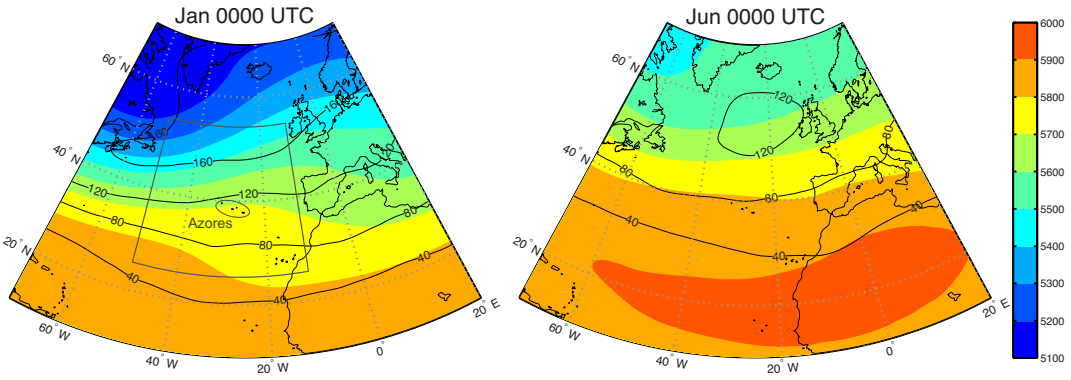

Figure 4.3 Mean 500-mb heights for January and June. The inner box in the top map represents the smaller domain used to explore variability in the vicinity of the Azores. Black contour lines are standard deviation of the mean 500-mb height, and can be used as a proxy for storm track variability, where higher numbers indicate higher variability.

4.1 June

Dominant synoptic states and environmental properties

The SOM nodes calculated for June are presented in Figure 4.4 as the positive (solid lines) and negative (dashed lines) anomalies overlaid on the mean 500-mb geopotential heights mapped to each node (we refer to these as "projected" quantities). A continuum ranging from almost entirely positive values (node 15), half positive and negative (nodes 23 and 3) and nearly all negative (node 11) is evident, although there are relatively equal distributions of positive and negative values across the entire SOM. The middle node (13) is characterized almost entirely by zero anomaly values, and thus represents (nearly) the climatological mean. SOM analysis (for all months) exhibit transitions around the edge states of the SOM, as synoptic patterns evolve from state to state. June experiences ridge like conditions a substantial amount of the time (21.7%, from Table 4.2, but also experiences a substantial amount of pre-trough (22.6%), trough (20.5%) and post-trough (25.2%) conditions. This meteorological variability is greater than the conditions understood from the patterns from the an-

nual SOM, where ridges are present 34.3% of the time.

By overlaying the normalized 500-mb geopotential height anomalies over the projected 500-mb geopotential heights, the meaning of the SOM structures becomes interpretable from a meteorological perspective. Positive anomaly structures correspond to conditions of higher-than-climatology pressure. For a somewhat zero-anomaly (climatology) state like that in June, nodes with positive anomaly values correspond to ridge-like structures, and negative anomaly values correspond to trough-like structures. The middle node (13) representing roughly the climatological mean shows the Azores just east of a very weak ridge axis and just very west of a weak trough axis. The corner nodes (5 and 21) are characterized by the most extreme synoptic structures, however, they are not the most frequent nodes in the June SOM. Nodes 15 and 11 are less extreme cases of the corner ridge and trough (5 and 21), and are two of the four most frequent June nodes. Nodes 15 and 11 both have axis features centered over the Azores. The Azores lie in a region of strong 500-mb geopotential height gradients in two other very frequent nodes (23 and 3). These nodes represent before and after the trough feature passes through the Azores.

Though the geopotential heights rarely drop below 5400-m, synoptic intrusions do occur over the Azores (e.g.,16, 11, and 6). The corners are more extreme cases of the middle-edge nodes, encompassing the classically-taught ridge and trough structure, and the middle-edge nodes are transitions between these extremes. Although the corner nodes contain the greatest anomaly values and strongest ridge and trough features, they are not the most frequent nodes, which actually lie on the middle-edges of the SOM, as indicated by the bold numbers on the upper left side of each node. The bold numbers represent statistically significant nodes using a 95% confidence interval for June. This suggests that June synoptic patterns typically embody less extreme cases of traditional ridges and troughs. Transitions between the more and

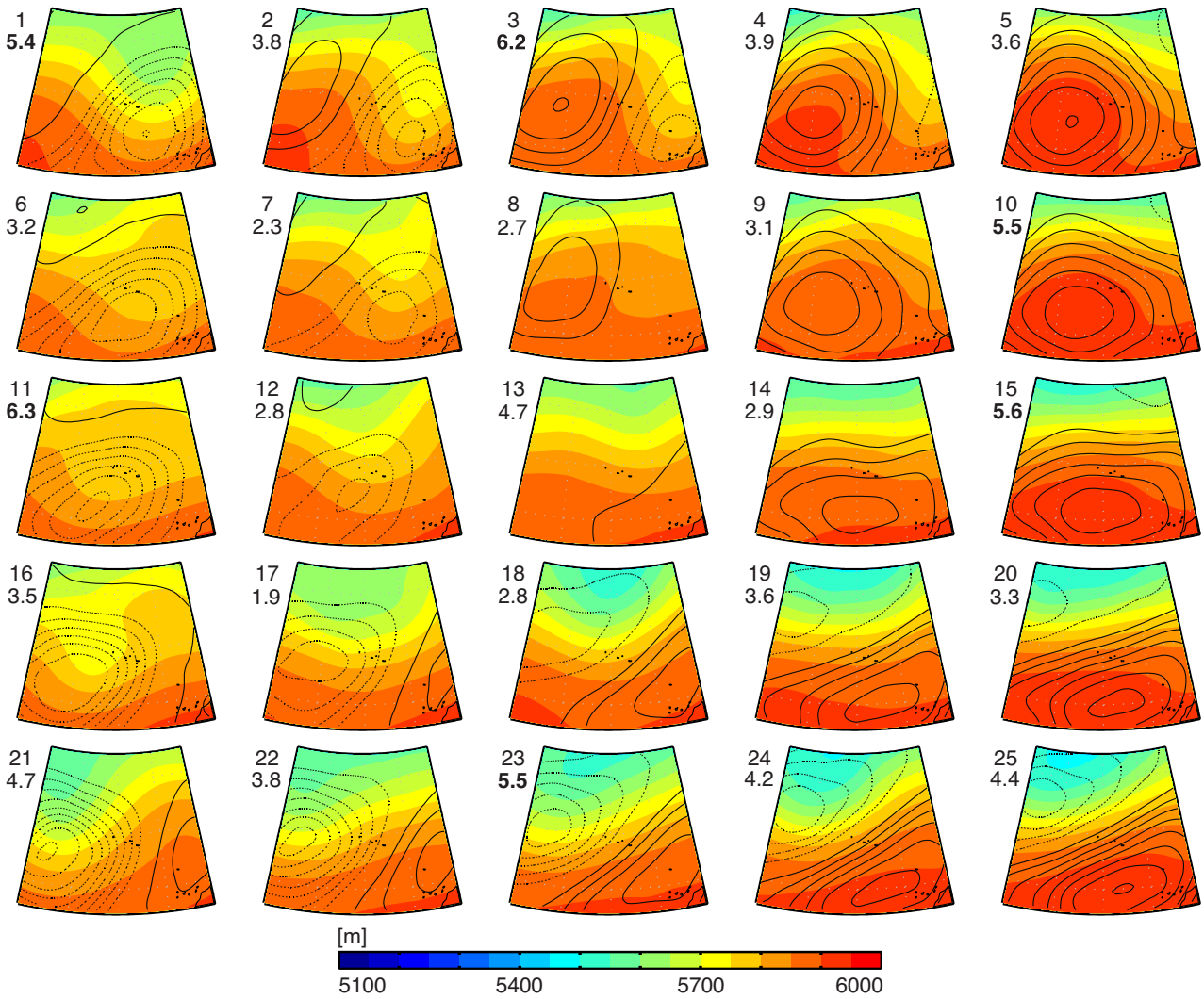

Figure 4.4 SOM nodes of 500-mb geopotential heights with overlaid gray contours of normalized anomaly 500-mb geopotential heights for June. Top numbers in upper left hand portion of each node indicate node number, while the bottom numbers indicate the relative frequency of occurrence of each node. Bold frequency values represent statistically significant nodes based on a 95% confidence interval. Dashed (solid) lines represent negative (positive) anomaly values.

less extreme nodes (see the Appendix) take place in a clockwise rotation around the SOM.

The most-frequent nodes found on the middle-edges represent the dominant, archetypal June synoptic patterns over the North Atlantic region. These dominant synoptic states and projected environmental properties of 500-mb geopotential heights, 1000-mb geopotential heights, 500-mb vertical velocity, and EIS are shown in Figure 4.5. We refer to these four dominant synoptic patterns as pre-trough, trough, post-trough, and ridge, based on the orientation of the synoptic pattern relative to the Azores.

The pre-trough pattern shows that the Azores lie in a tight gradient of 500-mb heights, with the trough axis near the western portion of the domain. At 1000-mb, a weak Bermuda High is present south and east of the Azores, and a low pressure center is present in the northwest portion of the domain. This 1000-mb trough is roughly co-located with the 500-mb trough axis. The Bermuda High is least spatially extensive across the domain in this state. The Bermuda High is least dominant in this synoptic state, reflected in the presence of the weak Icelandic Low, which happens to only be present in this pattern. An upward motion maximum at 500-mb is present downstream of the trough axis. EIS exhibits a tongue of low values oriented from southwest to northeast, with smaller values equatorward and to the west. This tongue of EIS values is present in all of the June dominant states, suggesting that differences within the month arise from sustained vertical motion acting on a baseline pattern of EIS. Areas of strong subsidence at 500-mb are associated with greater stability. The Azores experience low values of EIS in this pre-trough state, and lie on the border between upward and downward vertical motion at 500-mb, depending on the location of the trough axis at 500-mb.

The trough pattern shows a weak positively tilted upper-level trough located over

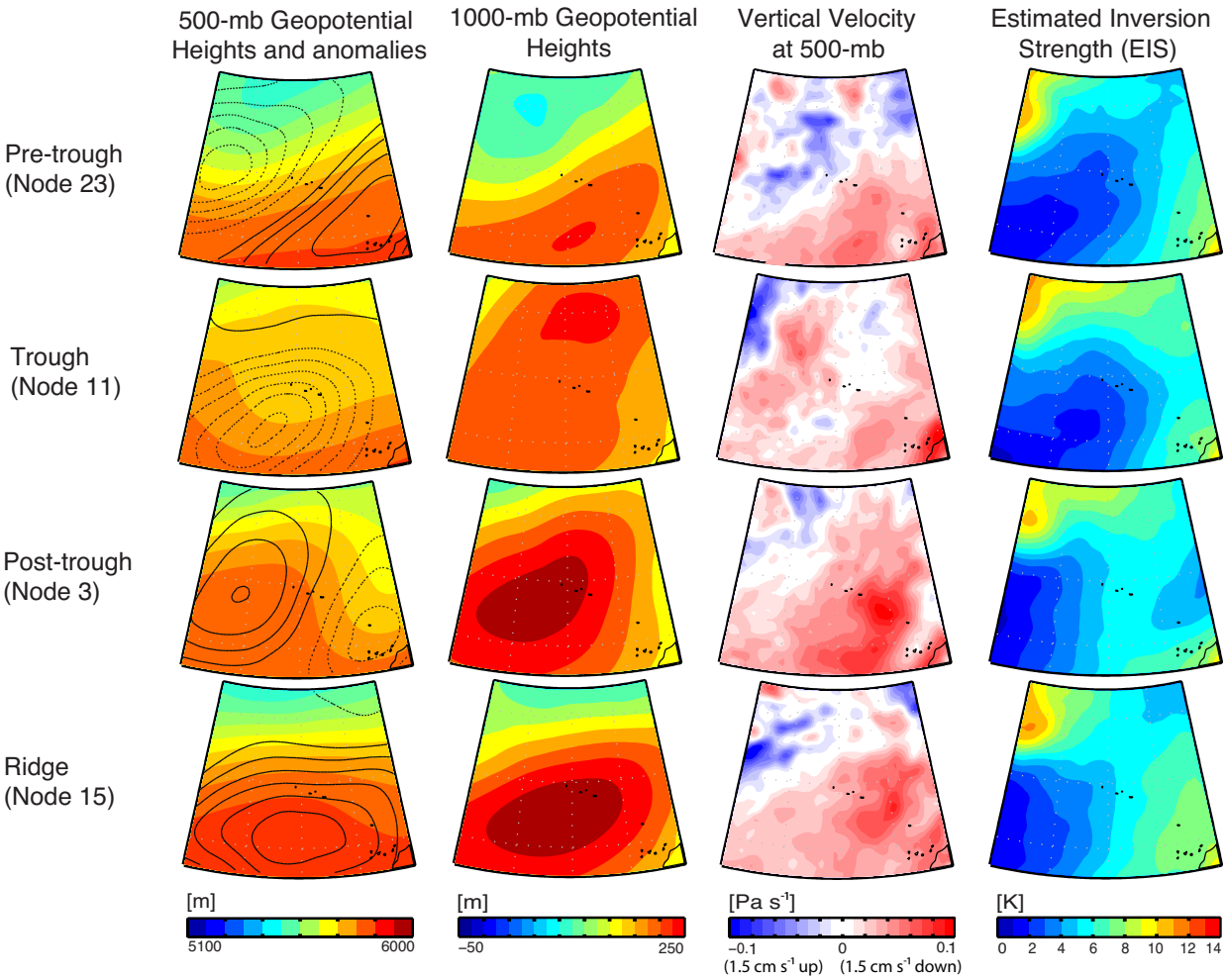

Figure 4.5 Synoptic properties for four patterns in June. These nodes are the highest frequency nodes and are interpreted as a representative for their relative synoptic patterns.

the Azores (indicated by the 500-mb heights). The upper-level trough is evidently not sufficiently strong to encourage a surface low to develop, but the pattern exhibits a weaker low-level Bermuda High that is present over most of the domain. The weak trough does not exhibit the robust region of ascent downstream of the trough axis as it is in the pre-trough pattern. Subsidence is widespread in this state, which has encouraged stronger stability values across the northern and and eastern portions of the domain (with the exception of the most northwestern portion of the domain,

which is strongly influenced by extremely cold waters, increasing stability in the area). The trough pattern exhibits EIS values similar to the pre-trough EIS values for the Azores.

The post-trough pattern shows the trough axis on the most eastern portion of the domain, with the Azores just east of a ridge axis. The Bermuda High is strong at this state, and is co-located below the 500-mb ridge axis. The small values in the EIS tongue are contained to the western portion of the domain, allowing for the majority of the eastern portion of the domain to be stable. The strongest subsidence is in this synoptic state, with a maximum located downstream of the 500-mb ridge axis. This strong subsidence promotes larger EIS values at the Azores compared to the pre-trough and trough states, and makes this the most stable synoptic state for the Azores. A region of low EIS values coexists with the trough axis on the farthest right portion of the domain.

The ridge pattern has the highest 500-mb heights for this month, with the ridge axis centered at the Azores. The Bermuda High at 1000-mb is similar to the structure in the post-trough state, but is more centered over the Azores and does not extend as far north. A stronger north-south gradient is present in both the 500-mb and 1000-mb geopotential height fields compared to the post-trough state. Subsidence dominates over much of the southern portion of the domain, with a maximum downstream of the ridge axis. The EIS structure is similar to the post-trough state, but the eastern potion of the domain is dominated by higher EIS values, due to sustained subsidence promoting stronger stability. The Azores lie in a fairly stable region as they do in the post-trough state.

Overall, the EIS structure is similar across the different patterns for June months, with a tongue of low values spreading from the southwest toward the northeast, extending through the middle of the domain. Sustained vertical motion over a region

modulates the changes in the EIS structure, where subsidence promotes stronger stability. Though most of the southeastern portion of the domain is dominated by continual subsidence, the Azores experience quite a bit of vertical velocity variability depending on the location of higher-latitude synoptic intrusions. June as a whole is dominated by the presence and persistence of the Bermuda High at lower levels, though synoptic intrusions do occur at higher levels during the pre-trough state.

Cloud Properties

The characteristic cloud patterns for the dominant June synoptic states are seen in Figure 4.6. Total condensate (LWP+IWP), total cloud fraction from ERA–Interim and MODIS, and cloud top temperature for ERA–Interim and MODIS are explored to understand cloud behavior for the dominant synoptic states. Past studies have successfully composited cloud properties for midlatitude cyclones (Field and Wood, 2007). Attempting to composite our ridge and trough-like nodes results in similar overall cloud structures, but the regions cloud regimes are difficult to distinguish (see Appendix), and it is thus important to examine individual nodes to avoid overgeneralized cloud regimes. Vertical bars between total condensate and ERA–Interim cloud fields represent the frequency of time that the Azores experience overcast (between 90 and 100%), overcast (between 10 and 89%), and clear (between 0 and 9%) conditions. These cloud fraction bars are a representation of the intranode variability experienced at the Azores.

In the pre-trough state, the majority of the domain is cloudy with the exception of the south to southwest regions. The area of high total condensate values to the northwest of the Azores coincide with areas of strong upward vertical motion from Figure 4.5. The corresponding band of clouds are visible on the reanalysis total cloud fraction and the cloud-top temperature from both reanalysis and MODIS. It is more

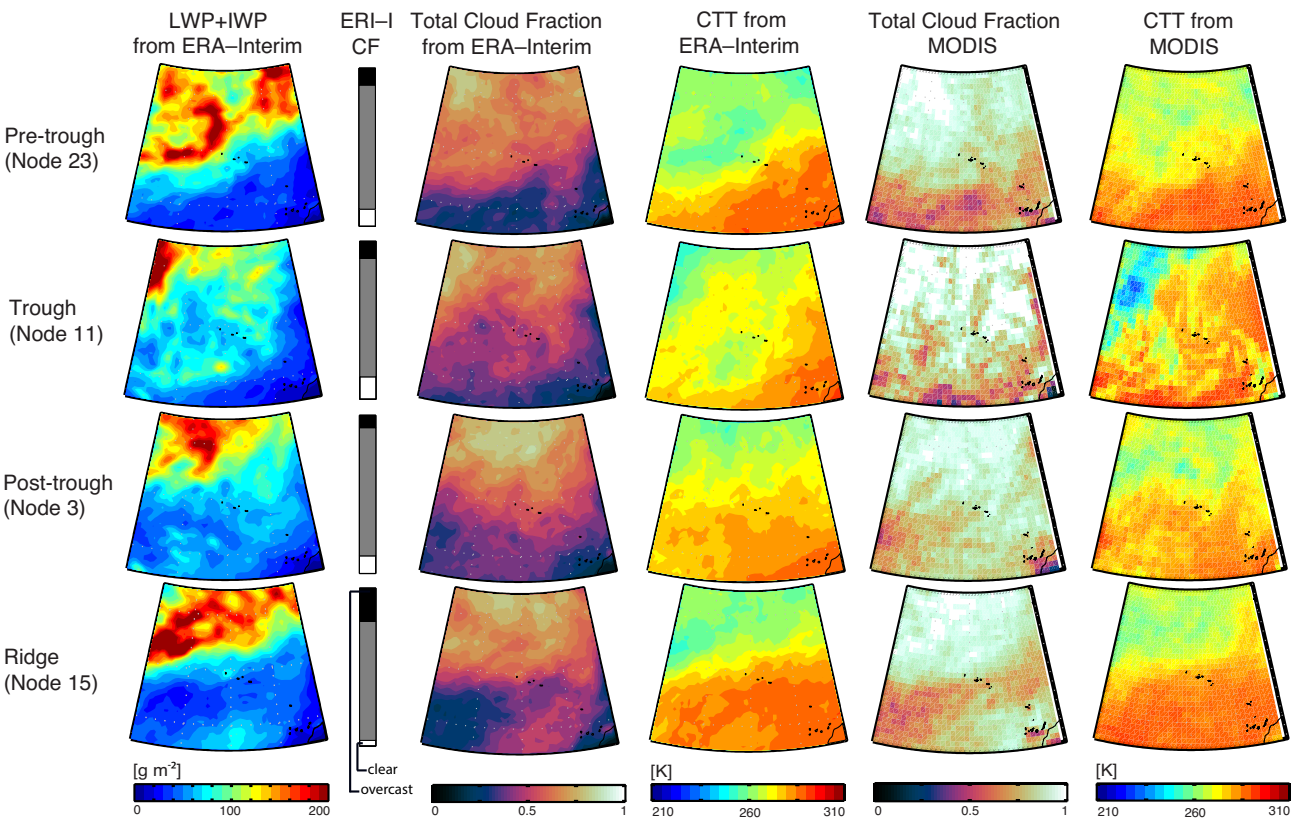

Figure 4.6 Cloud properties for four patterns in June.

difficult to distinguish this band of clouds from MODIS total cloud fraction because MODIS cloud fraction is systematically greater, and thus most of the domain looks cloudy. The location of this cloud band is downstream of the trough axis, where convective clouds and precipitation are usually expected to form. The clouds that coincide with high values of liquid condensate in the northwest portion of the domain can also be attributed to the strong upward motion at 500-mb. All of the cloud fields show a northwestern cloud structure with a sharp gradient from very cloudy in the northwest to nearly clear in the region south of the Azores. A strong gradient in vertical motion is also found along this gradient in cloud properties. To the southeast of the Azores, a cloud structure with lower cloud fraction and total condensate is evident in both reanalysis and MODIS, and covers the region to the east of the

Azores and extends south and slightly westward. These clouds lie in an area of subsidence and modestly stable values of EIS, but are not obvious in the cloud-top temperature fields, indicative of the low and warm nature of the Northern Atlantic stratocumulus deck. The western most portion of the stratocumulus deck reaches the eastern most island of the Azores chain. This stratocumulus deck is not as spatially extensive across the eastern ocean basin compared to other synoptic patterns that will be discussed. The Azores are wide enough to sample different cloud regimes in this state, depending on the exact location of the synoptic features.

The trough pattern shows the total condensate and ERA–Interim cloud fraction boundary displaced toward the southeast portion of the domain, with cooler reanalysis CTT covering most of the region. The gradients in cloud properties are not as strong in this state as they were in the pre-trough state, particularly in the vicinity of the Azores. This is possibly a reflection of a weaker gradient in vertical motion in this state from Figure 4.5. The reanalysis cold cloud tops along an axis from southwest of the Azores toward the northeast is loosely associated with a band of weak ascent or near-zero vertical motion, but this signal in CTT is not present in the MODIS retrievals, which indicate a substantial northward intrusion of warm cloud tops (low clouds). Although the reanalysis exhibits this CTT warm tongue over the eastern boundary of the domain, the warm cloud tops in MODIS cover a much greater area. The Azores experience a complex cloud regime in this state, but potentially for different reasons than the pre-trough state because the trough pattern is associated with interactions between the weaker northwestern cloud regime and the intrusion of low clouds.

In the post-trough state, total condensate is more extensive over the southern portion of the domain than in pre-trough and trough states. The area of strong subsidence in Figure 4.5 for this pattern indicates that the majority of the clouds over and to the east, south and southwest of the Azores are stratocumulus clouds. These

clouds have warmer cloud top temperatures for reanalysis and MODIS and larger CF on the MODIS total cloud fraction. These stratocumulus are found downstream of the 500-mb ridge axis on the eastern portion of the surface Bermuda High, in a region of stronger EIS values. The areas of maximum total condensate and reanalysis and MODIS cloud fraction are collocated with areas of ascent in the northwestern portion of the domain and do not reach as far south as in the pre-trough state. Stratocumulus are the dominant cloud type over the Azores in the post-trough state.

The ridge pattern most clearly illustrates the different cloud regimes in the region, due to the strong gradients in vertical motion and strong subsidence downstream from Figure 4.5. The area of ascent at 500-mb is associated with a continuous feature of total condensate values as high as 200 g m^{-2}, extending from the west of the Azores to the northeast portion of the domain. The clouds associated with this total condensate are cold (around 260 K for MODIS and reanalysis) and spatially extensive, with their boundary at the Azores. The Azores lie on the cloudy side of the boundary influenced by synoptic ascent, with the stratocumulus deck off to the east, southeast, and south. This stratocumulus deck is encouraged by the subsidence maximum in this state, and lies in an area of stronger stability. The stratocumulus deck is the most extensive in this ridge pattern, which may be attributed to such high values of subsidence downstream of the ridge axis. The Azores cloud conditions are thus influenced by the northern cloud regime, southeastern stratocumulus deck, and southwestern relatively clear slot, which may individually cover or overlap at the Azores. The overlapping of the regimes suggests an environment conducive to substantial variability in cloud properties at the Azores.

During June, individual or overlapping cloud regimes suggest great variability in cloud properties the Azores. In all of the synoptic states, a northwestern cloud regime associated with higher total condense values, higher CF (MODIS and reanalysis) and

colder CTT (MODIS analysis) values exists, as well as a southeast warm stratocumulus deck with smaller CF values and lower total condensate. The Azores are located in a prime region to experience both of the cloud regimes depending on the synoptic state. This suggests that the cloud conditions at the Azores extremely variable depending on exactly where the synoptic patterns are located.

4.2 January

Dominant synoptic states and environmental properties

For most synoptic patterns, the 500-mb gradient over the Azores is stronger in January and the heights are lower than June (as would be expected), seen in Figure 4.7. Geopotential heights are lower in winter than summer, with a range of 5100-5900 m in winter and 5400-6000 m in the summer. Note the wider range of values on average during the winter, indicative of stronger spatial gradients. The stronger north-south gradient in 500-mb geopotential heights causes the orientation of the normalized 500-mb geopotential height anomalies to become more horizontal compared to June. The upper level ridge is not as strong in January (node 5, Fig. 4.7) as in June (node 15, Fig. 4.4), while the trough is much greater amplitude (nodes 21-23 in Fig. 4.7 vs. node 11 in Fig. 4.4). The archetypal nodes for January are not as easy to distinguish as in June. In January, two of the highest frequency nodes lie on the corners of the SOM, while node 23 is a middle-edge node (and is largely a blend between 21 and 25). The two higher frequencies of the corner nodes suggests a synoptic structure in January that favors the more extreme synoptic states, and thus the corners are a natural choice for the archetypal states. The other corner nodes (1 and 21) do have high frequency values (4.9 and 4.6, respectively), even though they are not statistically significant. Though node 23 is more frequent than 21, node 21 still has a high frequency and they

are similar in nature except the trough axis is more centered over the Azores. Node 21 will thus be the trough pattern representative. The climatological state (node 13 in Fig. 4.7 and Fig. 4.3) has a diffluent trough structure, with east-west flow over the Azores.

January experiences much greater amounts of ridges than what was expected, with ridge like conditions present 25.4% of the time. There are also substantial occurrences of zonal conditions (17.1%), pre-trough (21.1%) and trough like conditions (17.2%).

The equivalent normalized anomaly structures for pre-trough, trough, post-trough and ridge synoptic patterns for January are seen in Figure 4.8, and these patterns show the dominant patterns for this month. Though the states have similar anomaly structures as the dominant synoptic June patterns, the projected quantities are very different in both magnitude and spatial distribution.

The pre-trough pattern for January has strong north-south gradients in 500-mb geopotential heights. The tight contours over the middle of the domain indicate a jet-like structure with a maximum in the middle of the domain. The trough axis is difficult to discern but lies west of the Azores. The 1000-mb structure resembles a confluent trough and also exhibits strong north-south gradients. Given the jet structure at 500-mb, the southwest and northeast regions of the domain constitute the right entrance and left exit regions, both regions of strong ascent, as reflected in the 500-mb vertical velocity field. The northwest and southeast portions of the domain are the left entrance and right exit regions, and lie under strong subsidence. The magnitude of vertical velocity in January is much greater than in June. South of the Azores has anticyclonic rotation from the Bermuda High while north has the Icelandic Low with cyclonic rotation, and the Azores are right in-between. The ascent in the left exit and right entrance regions are associated with smaller values of EIS. Stronger subsidence coincides with greater stability values in the right exit region.

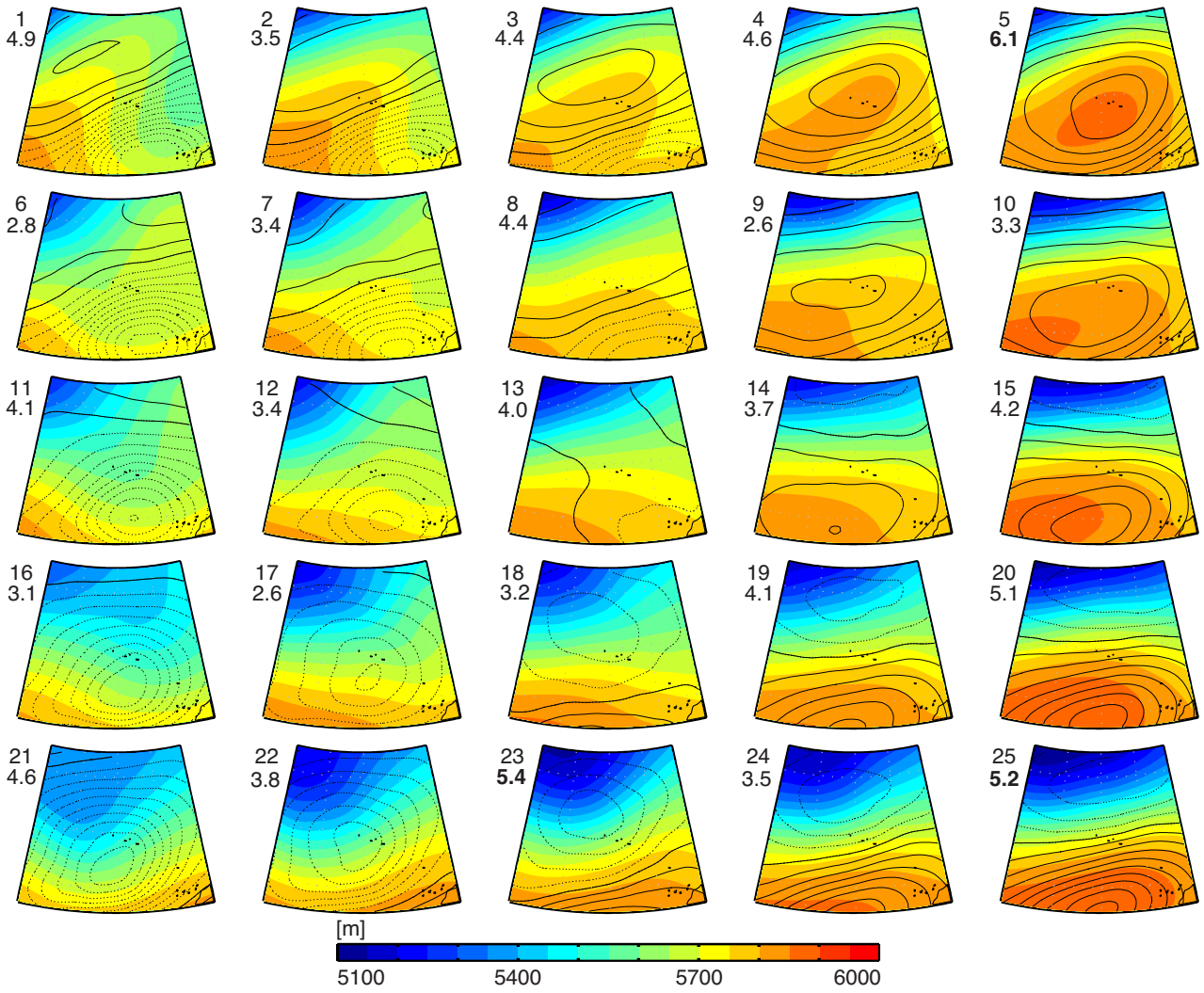

Figure 4.7 SOM nodes of 500-mb geopotential heights with overlaid gray contours of normalized anomaly 500-mb geopotential heights for January. Top numbers in upper left hand portion of each node indicate node number, while the bottom numbers indicate the relative frequency of occurrence of each node. Bold numbers indicate statistically significant nodes.

The most northwest regions of the domain experiences higher stability, though this is present in all of the synoptic patterns and in June as well because of the cold temperatures in this area. The baseline EIS tongue structure seen consistently in June is not found in January, when EIS varies much more. The Azores lie in a region of ascent and relatively low stability.

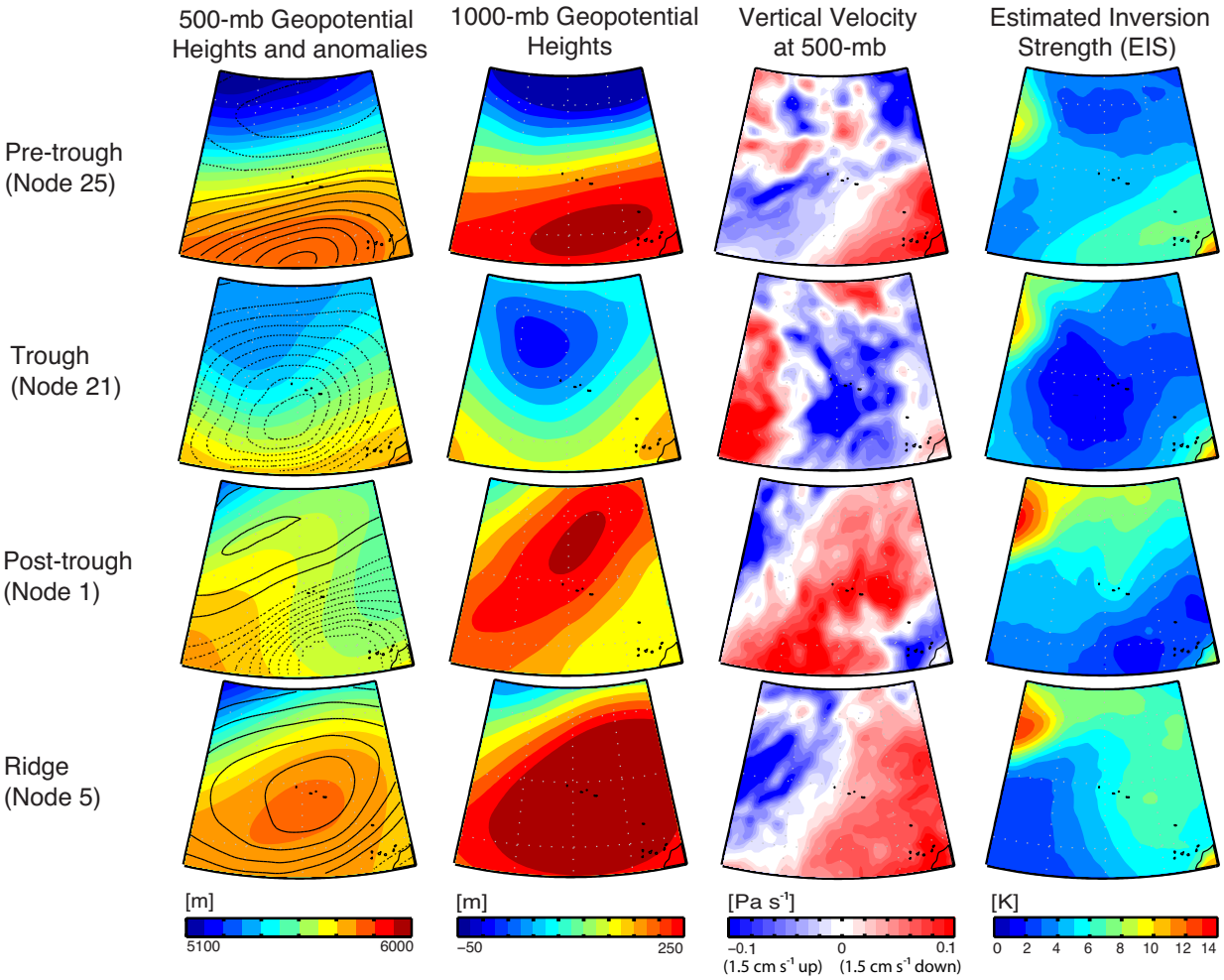

Figure 4.8 Synoptic properties projected for four patterns in January. The overall structure has greater north-south pressure gradients and more intense vertical velocity distributions. The 1000-mb height field contains values in excess of 250 m. The contour levels were chosen to accommodate the range of both summer and winter heights using the same contour limits and intervals.

The trough pattern has an easily distinguishable trough axis lying just west of the Azores. In this state, the Icelandic Low is the dominant feature at 1000-mb, and the Bermuda High is not present. The Icelandic Low is centered northwest of the islands, with its trough axis just downstream of the upper level trough axis. Most of center portion of the domain is dominated by strong ascent, but subsidence is present on the western and north-northeastern regions of the domain. This strongest ascent in

the center of the domain corresponds to the center of the lowest EIS values.

In the post-trough state, the trough is at the far eastern portion of the domain, and a weak, positively-tilted ridge is present over the western portion of the domain. The 500-mb ridge axis is oriented from the southwest to the northeast, and the trough axis is also positively tilted across the southeast corner of the domain. This positively-tilted ridge encourages the presence of an elongated Bermuda High, with its maximum directly north of the Azores. Strong subsidence is present over and downstream of the ridge axis, a region that is also characterized by high values of geopotential height at 1000 mb. Enhanced stability accompanies much of this large region of subsidence, and the Azores lies near a strong gradient in EIS. Low stability is found downstream of the trough axis in a region of ascent next to the African coastline.

A (relatively weak) 500-mb ridge is present in the ridge pattern centered over the Azores, with a slight Northeast-southwest tilt. 1000-mb heights show the presence of a strong Bermuda high, centered around and east of the Azores. This Bermuda High is intense and dominates most of the analysis domain. Subsidence is present over the eastern half of the High, particularly east of the ridge axis, while ascent is found on the western portion upstream of the ridge axis. The Azores lie in the boundary between the this couplet of vertical motion fields. This vertical velocity couplet feature appears to be associated with with a couplet feature in the EIS field, specifically the tongue/intrusion of low EIS to the west of the Azores and a region of high EIS to the east. High values of EIS are found in the northern and eastern portions of the domain. Large values of EIS are found in the region where stratocumulus decks tend to persist in summertime months. In January, however, subsidence and stability are even stronger and more spatially wide spread than in June.

The month of January shows much more variability across characteristic states than in June. Large-scale ascent associated with midlatitude synoptic systems reach

lower latitudes in winter, allowing the lower latitudes to experience sustained periods of large-scale ascent. The vertical velocity fields are much stronger as a whole, and the Azores lie in the boundary between vertical motion fields in multiple synoptic patterns (pre-trough and ridge). The Icelandic Low exerts a strong influence during wintertime months, which seems to be the ultimate source of a lot of meteorological variability across the patterns, as the low develops and modulates the strength and persistence of the Bermuda High.

Cloud Properties

The characteristic cloud properties associated with each characteristic synoptic pattern for January are seen in Figure 4.9. The structures exhibit more variation across the pattern than the characteristic patterns for June.

In the pre-trough state, nearly the whole domain is cloudy for both reanalysis and MODIS, except for the most southeast and southwest regions. The total condensate field shows a strong gradient across the Azores. A local maximum in total condensate in the northeast portion of the domain associated with the strong ascent from the left exit region of the jet-like structure in this synoptic pattern from Figure 4.8. ERA–Interim and MODIS show similar structures across the domain, but as previously seen, MODIS cloud fractions are larger than those from reanalysis. Large values of cloud fraction prevail across most of the domain, but differences in cloud-top temperature between MODIS and reanalysis suggest differences in cloud type and behavior. The coldest clouds in the reanalysis CTT are in the area of ascent and are located in the northern portions of the domain, extending down to the Azores. In the middle of the most southern portion of the domain, however, clouds are present in both the total condensate and total cloud fraction for reanalysis and MODIS that are not distinguishable from the reanalysis or MODIS CTT. These must be stratocumu-

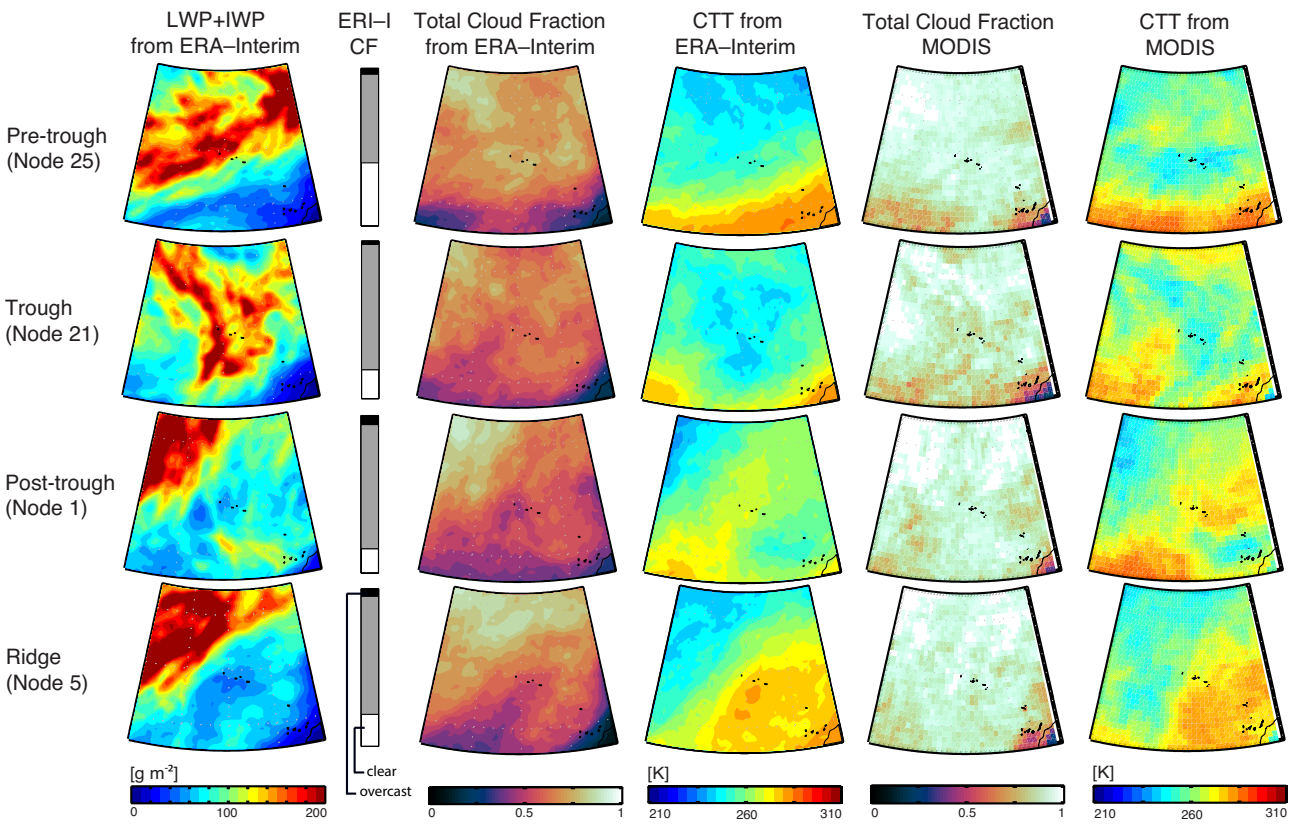

Figure 4.9 Cloud properties for four patterns in January.

lus because of their warm CTT values (around 280K), higher CF (close to 1.0 from MODIS), and lower total condensate values (around 60 g m^{-3}).

The cloud structure in the trough pattern changes to a more north-south orientation, located just east of the trough axis in Figure 4.8, as seen in the total condensate. These large values of condensate are also associated with the location of strong ascent and low stability values. Cold clouds for both MODIS and reanalysis within this region of strong ascent are distinguishable from the CTT images, and are centered over the Azores. This band of cold cloud tops, however, is more narrow in MODIS than in the reanalysis. Following behind the condensate structure in the reanalysis, a region of lower cloud fraction exists to west of the trough axis where subsidence is present in Figure 4.8. These clouds are warmer than those in the ascent region around the

Azores, and could be a trailing stratocumulus region. The cloud property structures (particularly total condensate and MODIS CTT) are strikingly similar to the vertical velocity field.

In the post-trough state, the northwestern clouds are strongly tied in the region of ascent upstream of the ridge axis in Figure 4.8. In the southeast, a pocket of cold clouds in a region of ascent downstream of the trough axis is present in reanalysis and MODIS. The area between the northwestern cloud regime and the southeast cold pocket is comprised of warmer clouds in a region of subsidence, suggesting stratocumulus. These clouds cross a strong gradient from weaker to stronger EIS, which is an interesting feature in this post-trough state, where other states have stratocumulus in regions associated with consistently strong stability values. These clouds are consistent with the post-cold-frontal stratocumulus seen in Mechem et al. (2010).

The January ridge state, as in June, exhibits two well defined cloud regimes seen in the reanalysis total condensate and reanalysis and MODIS cloud-top temperature. These cloud regimes are the northern arctic clouds and the eastern ocean basin clouds. A distinct couplet of these cloud types is associated with the vertical velocity and stability couplets from Figure 4.8. The northwest, which is dominated by ascent, has widespread cold clouds and total condensate values of 200 g m^{-2}. Cold cloud-top temperatures of around 260 K extend to the Azores. In the ascent region associated with higher stability downstream of the ridge axis in Figure 4.8, warmer cloud top temperatures and lower total condensate values persist, suggesting stratocumulus. These stratocumulus are in the same region as the June ridge pattern and have similar spatial coverage. The Azores are again in a region of overlapping cloud regimes.

The common theme across the synoptic patterns in January is one of prevalent cloudiness, but details of cloud structure differ. Much greater variability in magnitude and spatial distribution of the environmental properties are present in January,

due to the modulation of the Bermuda High by the Icelandic Low. The location of stratocumulus is encouraged from the locations of subsidence in the 500-mb vertical velocity field. The Azores in January, as in June, lie in a region of overlapping cloud types and thus exhibit substantial variability in cloud properties.

4.3 Joint variability of cloud fraction with vertical motion and EIS

After examining the spatial distribution of environmental and cloud properties for the dominant synoptic states in January and June, an exploration of potential relationships between cloud fraction and synoptic properties may further the understanding of cloud cover at the Azores. Past studies have examined the relationship between low-cloud fraction and stability on seasonal timescales. KH93 examined low-clouds with LTS through seasonal averages of cloud fraction and stability at various locations around the globe, and established a positive relationship, with an r^2 value of 0.884 and a slope of 5.7. Wood and Bretherton (2006), WB06 hereafter, established EIS as an estimate for the inversion strength, and explored the relationship between low-level cloud fraction and EIS. They also found an even stronger positive relationship between cloud fraction and EIS with an r^2 value of 0.92. Both studies established a simple linear function to describe the relationship between the stability values and cloud fraction, based on values representative of seasonal means. Here, we explore the possible correlations between instantaneous cloud fraction and synoptic properties for January and June, and then composite the relationships by synoptic regime.

The joint probability distribution functions (PDF) of ERA–Interim cloud fraction and EIS for January and June are seen in the far left column in Figure 4.10. Note that the correlation is calculated for the total cloud fraction, not low-level cloud

fraction as it was in KH93 and WB06. The WB06 linear relationship is overlaid with a dashed line on the June cloud fraction and EIS plot. A strong relationship is not easily distinguishable between cloud fraction and EIS, if at all, between these two fields on the daily timescale. The correlations from the composited data for synoptic state for January and June are seen in the right four columns in Figure 4.10. Still, a correlation is not easily distinguished, suggesting that a robust relationship is not present between CF and EIS, at least not on short timescales.

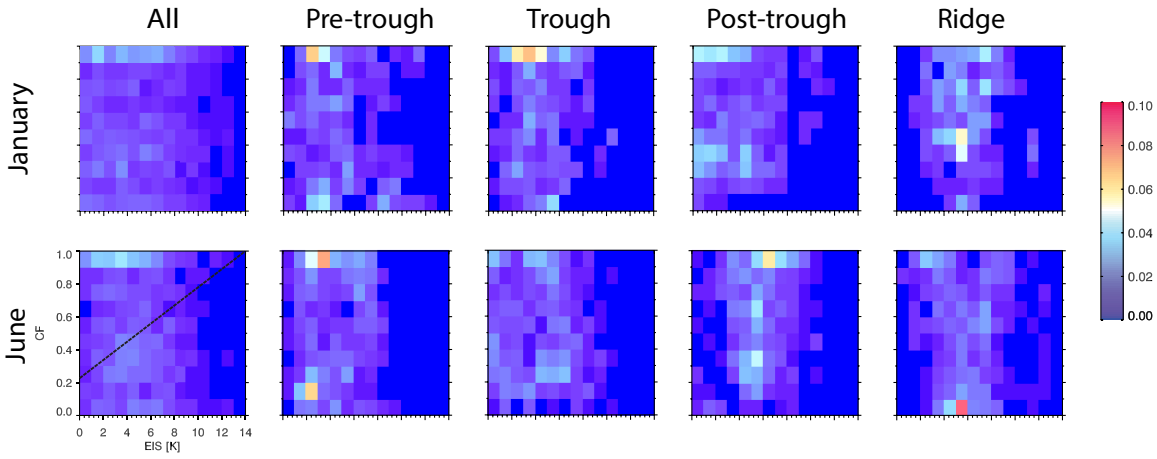

Figure 4.10 Joint PDFs of cloud fraction and EIS for the entire monthly data sets (All) and for each archetypal synoptic pattern for both June and January. The dashed line shows the EIS versus low-cloud amount found in Wood and Bretherton 2006 A correlation is not clear for the entire monthly data sets or when broken down into synoptic state.

The synoptic projections for January and June suggest that sustained vertical velocity modulate the baseline EIS values and and the vertical motion field has a more striking resemblance to cloud structures. For this reason we calculate the joint PDF for cloud fraction and vertical velocity, shown in Figure 4.11. The entire monthly data sets for January and June cloud fraction and vertical velocity does not show a robust correlation. Calculating the correlation from the composited data for each pattern does not reveal much of a relationship either. A subtle negative slant is

distinguishable in the trough and post-trough patterns, where higher cloud fraction is associated with stronger values of ascent. This subtle tilt is consistent with the expected synoptic behavior for such trough and post-trough states. Although the projected vertical velocity and cloud fraction properties for the SOMs bear a striking resemblance, these PDFs suggest that a robust relationship between the variables cannot be established on daily timescales, even when composited by synoptic state.

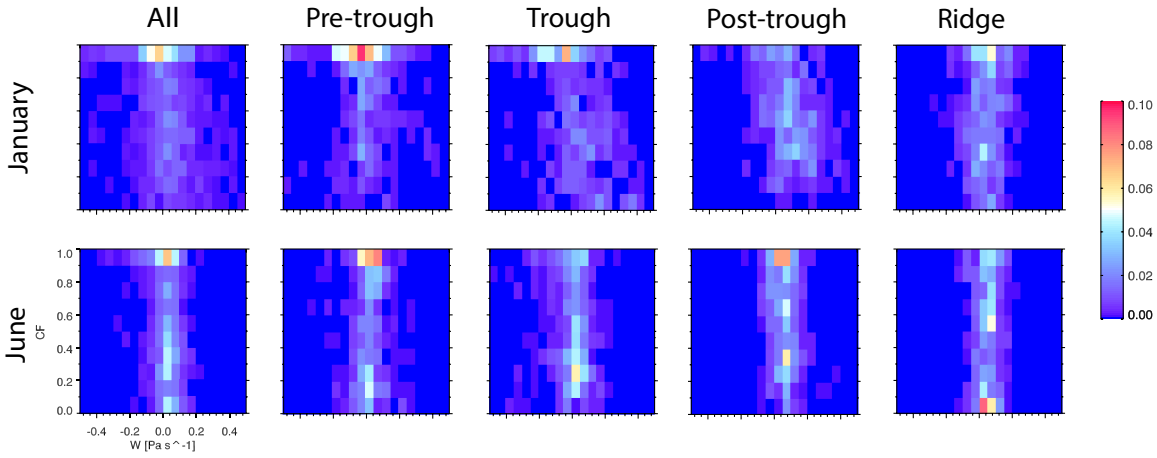

Figure 4.11 Joint PDFs of cloud fraction and vertical velocity for the entire monthly data sets (All) and calculated for the composited synoptic patterns for both June and January. No correlation is found when calculated over the entire data set for each month.

Chapter 5

Conclusion

The technique of self-organizing maps (SOMs) was employed to develop a climatology of synoptic and cloud patterns centered on the Azores islands in the Northeast Atlantic. The SOM technique proved successful in identifying these dominant synoptic states for June and January, establishing an understanding of not only summer and winter months individually, but providing broad insights into the annual cycle of synoptic and cloud properties. The second and more primary goal of understanding the projected cloud and environmental properties for the dominant synoptic states was also explored. The Azores consistently lie in an area of substantial variability in both synoptic configuration and environmental and cloud properties.

A surprising amount of synoptic intrusions are experienced at the Azores in June (20.5% of the time). Also, a substantial frequency of ridge like conditions were experienced in January (25.4% of the time), which provide conditions supportive to the formation of stratocumulus. Much greater variability in synoptic patterns within each month is experienced when the SOMs are calculated for each individual month, as opposed to calculating the SOM over the annual cycle. This substantial within month variability supported a closer examination of individual months, in which January

and June are highlighted.

The dominant synoptic states were established for January and June, providing a spatial understanding of the behavior of environmental and cloud properties in the region. Ridges, troughs, and transitional patterns are present for both months, but they must be understood individually to grasp the magnitude and orientation of summer versus winter ridge patterns, for example. Since the analysis is based on anomalies, frequencies cannot be compared across months. The use of anomalies essentially performed a high-pass filter, which filters out the low-frequency (seasonal) variability, leaving the short-term synoptic variability. We interpret higher-frequency nodes as archetype synoptic patterns. Performing the analysis on a month-by-month basis accentuates the synoptic variability relevant for that particular month.

The Bermuda High is present in all synoptic states in June but is most dominant in the ridge and post-trough states. For synoptic patterns in which the Bermuda High is weaker, synoptic intrusions at higher latitudes are permitted into the domain, as evinced by the weak trough in the trough synoptic state. This trough pattern is associated with a weaker, spread out Bermuda High at lower levels. When an upper level ridge over the Bermuda High is present with the ridge axis centered over the Azores, associated subsidence conditions east and southeastward of the Azores create a prime region for the persistence of stratocumulus cloud decks. The baseline tongue structure of EIS is modulated by sustained vertical velocity fields, where subsidence is associated with increased stability. The stratocumulus decks are therefore dominant in regions with sustained subsidence and higher stability values, located downstream of a ridge axis. The western most border of this cloud deck reaches the Azores. The Azores at times exhibits both the northern, cold, thick cloud regime as well as the warmer stratocumulus deck. This highly variable nature of the clouds at the Azores are attributed to these overlapping cloud regimes.

Summertime months have the highest amounts of low-level clouds at the Azores, which are predominantly associated regions of subsidence in ridge and post-trough patterns. June does not see the extreme forms of troughs and ridges found on the corner of the SOM as frequently as its less extreme states on the middle-edges of the SOM. The Azores experience an advance and retreat of more northern, high-level clouds, as well as slight eastward and westward shifts of the stratocumulus deck, creating a sloshing back and forth between the two cloud regimes with potential for overlapping cloud properties at the Azores.

January offers a different environment, with greater spatial variability in the region in cloud and environmental properties. Instead of large-scale flow controlled by the strength and persistence of the Bermuda High, the development of the Icelandic low modulates the High in the trough and post-trough states. This Icelandic Low influence causes great differences in cloud regimes between states, particularly in the trough and post-trough states. The post-trough state even exhibits a post-cold-frontal stratocumulus cloud regime found in previous studies (Mechem et al., 2010). January, like June, also exhibits the subsidence-dominated stratocumulus regime. That said, the state with the most dominant low-level clouds is still the ridge pattern, persisting in the region of subsidence southeast of the Azores, just like June. The pre-trough pattern exhibits many of the characteristics of zonal flow, but looking at cloud properties reveals a clear frontal cloud structure approaching the Azores.

Correlations between cloud fraction and vertical velocity and EIS on daily timescales for each month offered no relationship of joint variability. Calculating the joint variability by each dominant state, did not reveal a robust relationship either. The relationships established between stability and low-cloud fraction in past studies (KH93 and WB06) were calculated for seasonal averages, and robust relationships were established. The lack of relationship in the present study is attributed to the fact that

we are examining the correlations on a daily timescale, not a seasonal time scale. This is because the relationships do not hold for instantaneous time scales, but instead require sustained environmental properties over longer time scales to encourage an environment with a strong enough inversion and the build up of low-level moisture that is suitable for persistent low-level cloud coverage.

The findings of this study support the first hypothesis that synoptic intrusions do occur from higher latitudes in summer months. January exhibits the greatest variety of flow patterns, both in extremes of magnitude but also variations spatially. The locations of stratocumulus decks agree with Norris and Klein (2000) findings of where they should be located, regions of subsidence and (to the east of) a surface ridge. Though it may be of value to look at all of the generated SOM nodes for each month, the nodes shown in this study achieved the goal of depicting the primary conditions summer and winter in the Northern Atlantic region, specifically the Azores.

A permanent campaign in the Azores would benefit from a climatological understanding of the environmental and cloud properties in this highly variable region. A synoptic classification of meteorological patterns shows that the Azores lie in a strong gradient of atmospheric and cloud properties, with opposing vertical velocities and overlapping cloud regimes commonplace for the Azores. This variability suggests that the Azores should not be taken as a singular representation for the cloud conditions in the NEA without first considering the meteorological features within the region. The main takeaway points are as follows:

1. The SOM technique can successfully identify the full range of synoptic regimes.

2. Stratocumulus are most commonly found downstream of a ridge axis in areas of sustained subsidence and persistent high stability.

3. The Azores experience regular synoptic intrusions, even during the warm season.

4. January exhibits a substantial frequency of stratocumulus occurrence.

5. Vertical velocity modulates EIS so that sustained subsidence is associated with enhanced stability.

6. Patterns of vertical motion and cloud fraction are strikingly similar but exhibit very little robust statistical correlation due to calculations on daily time scales.

7. Most importantly, the Azores lie in a region of overlapping meteorological and cloud regimes.

5.1 Appendix

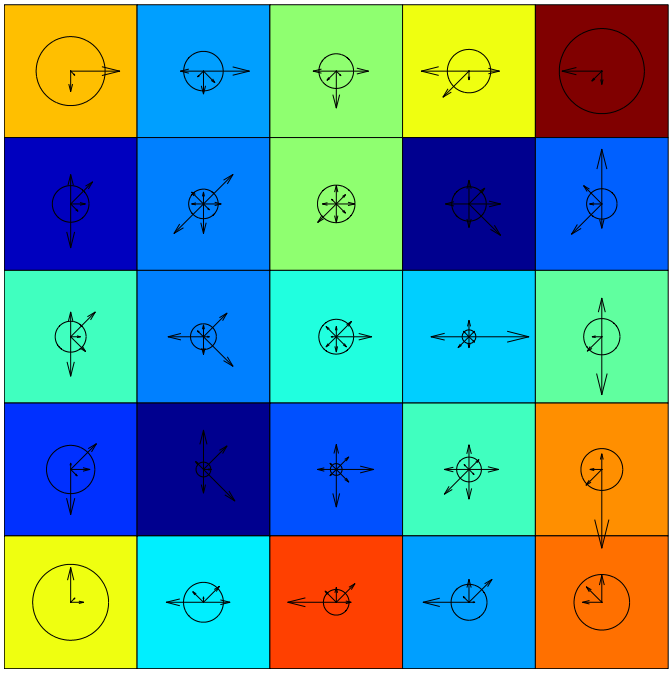

Figure 5.1 January forward trajectories show the transitions from node to node, with arrows showing where the next successive data sampled is plotted. The circles indicate how many times a data sample has been mapped in a row, showing how persistent the node is. Corner nodes are the most persistent, implying that data tend to stay in these nodes for lengthy amounts of time.

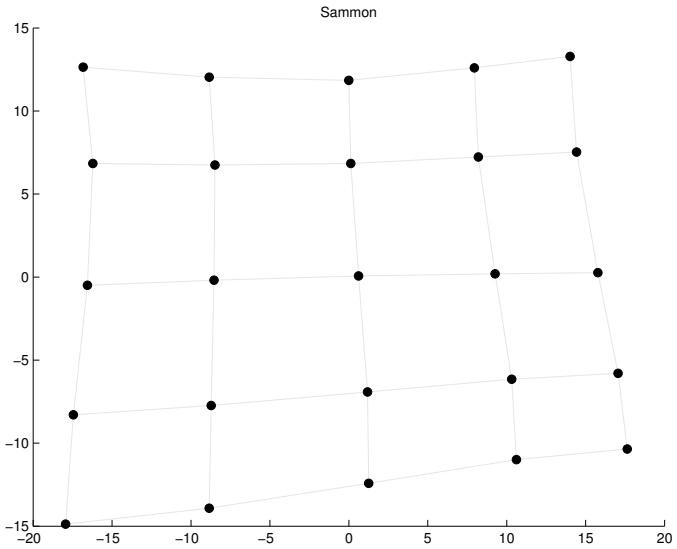

Figure 5.2 Sammon Map shows the relative locations of nodes to each other. Nodes in the upper right and lower right corners are more similar to each other than the lower left corner. The interior nodes are the furthest apart from each other.

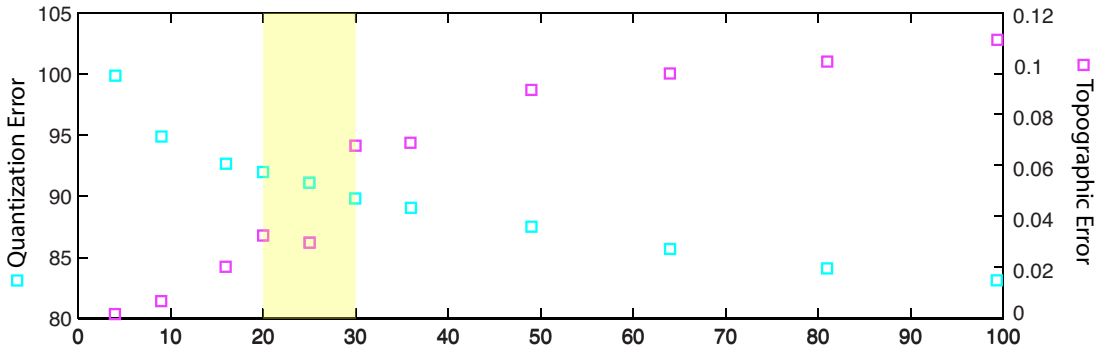

Figure 5.3 Elbow plot used to show how optimal number of nodes are chosen. Quantization error decreases with increasing number of nodes while topographic error increases with increasing number of nodes. The optimal number chosen is 25 nodes, highlighted in the region shaded with yellow.

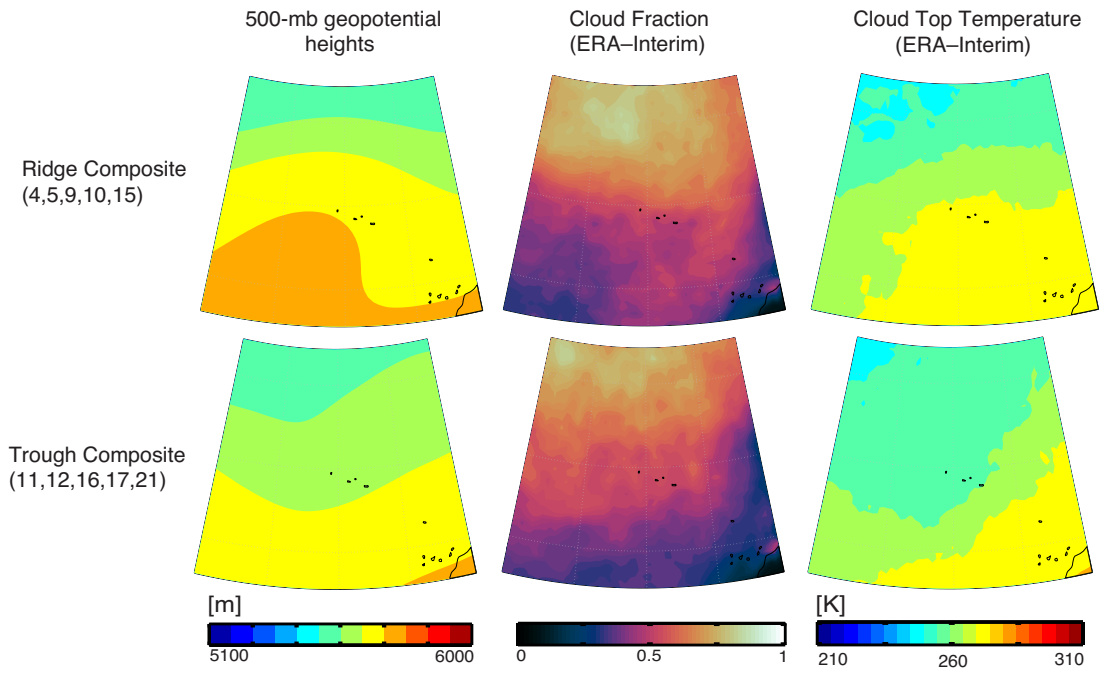

Figure 5.4 An example of composited 500-mb geopotential height and ERA–Interim total cloud fraction and CTT values for ridge and trough like nodes in June. Nodes used to composite these figures are shown under the pattern names. Though the patterns generally resemble the structures in the corresponding projected environmental and cloud quantities, the cloud structures are much less defined and the geopotential heights are less intense in magnitude.

Bibliography

Abercromby, R., 1883: On certain types of British weather. *Q. J. R. Meteorol. Soc.*, **9**, 1–25.

Albrecht, B. A., C. S. Bretherton, D. Johnson, W. H. Schubert, and A. S. Frisch, 1995: The atlantic statocumulus experiment — ASTEX. *Bull. Amer. Meteor. Soc.*, **76**, 889–904.

Albrecht, B. A., D. A. Randall, and S. Nicholls, 1988: Observations of marine stratocumulus clouds during fire. *Bull. Amer. Meteor. Soc.*, **69**, 618–626.

Ambroise, C., F. Badran, and S. Thiria, 2000: Hierarchical clustering of self-organizing maps for cloud classification. *Neurocomputing*, **30**, 47–52.

Bailey, A., T. N. Chase, J. J. Cassano, and D. Noone, 2011: Changing temperature inversion characteristic in the u.s. southwest and relationships to large-scale atmospheric circulation. *J. Appl. Meteor. Climatol.*, **50**, 1307–1323.

Barry, R. G. and A. H. Perry, 1973: Synoptic climatology: Methods and applications. *J. Appl. Meteor. Climatol.*

Bony, S. and J. Dufresne, 2005: Marine boundary layer clouds at the heart of tropical cloud feedback uncertainties in climate models. *Geophys. Res. Lett.*, **32**, L20 806, doi:10.1029/2005GL023851.

Bretherton, C. S., et al., 2004: The EPIC 2001 stratocumulus study. *Bull. Amer. Meteor. Soc.*, **85**, 967–977.

Cassano, E. N., A. H. Lynch, J. J. Cassano, and M. R. Koslow, 2006: Classification of synoptic patterns in the western Arctic associated with extreme events at Barrow, Alaska, USA. *Clim. Res.*, **30**, 83–97.

Cavazos, T., 2000: Using self-organizing maps to investigate extreme climate events: An application to wintertime precipitation in the Balkins. *J. Clim.*, **13**, 1718–1732.

Crane, R. G., 1978: Seasonal variations of sea ice extent in the Davis Strait-Labrader Sea area and its relationships with synotpic-scale atmospheric circulation. *Arctic*, **31**, 437–447.

Dee, D. P. w. . c.-a., 2011: The erainterim reanalysis: configuration and performance of the data assimilation system. *Quart. J. R. Meteoro Soc*, **137**, 553–597.

Field, P. R. and R. Wood, 2007: Precipitation and cloud structure in midlatitude cyclones. *J. Climate*, **20**, 233–254; Corrigendum, **20**, 5208.

Folland, C. K., J. Knight, H. W. Linderholm, D. Fereday, S. Ineson, and J. W. Hurrell, 2009: The summer North Atlantic Oscillation: Past, present, and future. *J. Climate*, **22**, 1082–1103.

Gong, D. and S. Wang, 1999: Definition of antarctic oscillation index. *Geo. Res. Lett.*, **26**, 459–462.

Hartmann, D. L., M. E. Ockert-Bell, and M. L. Michelsen, 1992: The effect of cloud type on earth's energy balance-global analysis. *J. Climate*, **5**, 1281–1304.

Hewitson, B. C. and R. G. Crane, 1994: *Neural computing: applications in geography.* Kluwer Academic Publishers, Dordrecht.

Hewitson, B. D. and R. G. Crane, 2002: Self-organizing maps: applications to synoptic climatology. *Clim. Res.*, **22**, 13–26.

Klein, S. A., 1997: Synoptic variability of low-cloud properties and meteorological parameters in the subtropical trade wind boundary layer. *J. Climate*, **10**, 2018–2039.

Klein, S. A. and D. L. Hartmann, 1993: The seasonal cycle of low stratiform clouds. *J. Climate*, **6**, 1587–1606.

Klein, S. A., D. L. Hartmann, and J. R. Norris, 1995: On the relationships among low-cloud structure, sea surface temperature, and atmospheric circulation in the summertime northeast pacific. *J. Climate*, **8**, 1140–1155.

Kohonen, T., 1990: The self-organizing map. *Proceedings of the IEEE.*, **78**, 1464–1479.

Köppen, W., 1874: *Über die Abhängigkeit des klimatischen Charakters der Winde von ihrem Ursprunge*. Methuen & Co Ltd., London, cited from Barry and Perry (1973).

Lamb, H. H., 1950: Types and spells of weather around the year in the british isles: annual trends, seasonal structure of the year, singularities. *Q. J. R. Meteorol. Soc.*, **76**, 393–429.

Li, W., L. Li, R. Fu, Y. Deng, and H. Wang, 2011: Changes to the North Atlantic subtropical high and its role in the intensification of summer rainfall variability in the Southeastern United States. *J. Climate*, **24**, 1499–1506.

Lilly, D. K., 1968: Models of cloud-topped mixed layers under a strong inversion. *Quart. J. Roy. Meteor. Soc.*, **94**, 292–309.

Mechem, D. B., Y. L. Kogan, and D. M. Schultz, 2010: Large eddy observations of post-cold-frontal continental stratus. *J. Atmos. Sci.*, **67**, 3368–3383.

Medeiros, B., B. Stevens, I. M. Held, M. Zhao, D. L. Williamson, J. G. Olson, and C. S. Bretherton, 2008: Aquaplanets, climate sensitivity, and low clouds. *J. Climate*, **21**, 4974–4991.

Morcrette, J. J. and Y. Fouquart, 1986: The overlapping of cloud layers in shortwave radiation parameterizations. *J. Atmos. Sci.*, **43**, 321–328.

Norris, J. R., 1998: Low cloud type over the ocean from surface observations. part i: Relationship to surface meteorology and the vertical distribution of temperature and moisture. *J. Climate*, **11**, 369–382.

Norris, J. R. and S. A. Klein, 2000: Low cloud type over the ocean from surface observations. part iii: Relationship to vertical motion and the regional synoptic environment. *J. Climate*, **13**, 245–256.

Oreopoulos, L. and M. Khairoutdinov, 2003: Overlap properties of clouds generated by a cloud-resolving model. *J. Geo. Res.*, **108**, 4479–4488.

Paluch, I. R. and D. H. Lenschow, 1991: Stratiform cloud formation in the marine boundary layer. *J. Atmos. Sci.*, **48**, 2141–2158.

Platnick, S., M. D. King, S. A. Ackerman, W. P. Menzel, B. A. Baum, J. C. Ridi, and R. A. Frey, 2003: The modis cloud products: Algorithms and examples from terra. *IEEE Transactions on geoscience and Remote Sensing*, **41**, 459–473.

Rémillard, J., P. Kollias, E. Luke, and R. Wood, 2012: Marine boundary layer cloud observations in the Azores. *J. Climate*, **25**, 7381–7398.

Rossow, W. B. and R. A. Schiffer, 1999: Advances in understanding clouds from ISCCP. *Bull. Amer. Meteor. Soc.*, **80**, 2261–2288.

Schubert, W. H., 1976: Experiments with lilly's cloud-topped mixed layer model. *J. Atmos. Sci.*, **33**, 436–446.

Schuenemann, K. C., J. J. Cassano, and J. Finnis, 2009: Synoptic forcing of precipitation over Greenland: Climatology for 1961-99. *J. Hydrometeor*, **10**, 60–78.

Stevens, B., et al., 2003: Dynamics and chemistry of marine stratocumulus — DYCOMS-II. *Bull. Amer. Meteor. Soc.*, **84**, 579–593.

Tibshirani, G., G. Walther, and T. Hastie, 2001: Estimating the number of clusters in a data set via the gap statistic. *J. R. Statist. Soc*, **63**, 411–423.

Tselioudis, G., W. Rossow, Y. Zhang, , and D. Konsta, 2013: Global weather states and their properties from passive and active satellite cloud retrievals. *J. Climate*, **26**, 7734–7746.

Warren, S. G., C. J. Hahn, J. London, R. M. Chervi, and R. L. Jenne, 1986: *Global Distribution of Total Cloud Cover and Cloud Type Amounts over the Ocean*. Tech. rep., NCAR Technical Note TN–317+STR, Boulder, CO, 42 pp. + 170 maps (also DOE/ER–0406). Available from Carbon Dioxide Information Analysis Center, Oak Ridge, Tennessee.

Wood, R., 2012: Stratocumulus clouds. *Mon. Wea. Rev.*, **140**, 2373–2423.

Wood, R. and C. S. Bretherton, 2006: On the relationship between stratiform low cloud cover and lower-tropospheric stability. *J. Climate*, **19**, 6425–6432.

Wood, R., et al., 2011: The VAMOS Ocean–Cloud–Atmosphere–Land Study Regional Experiment (VOCALS–REx): Goals, platformas, and field operations. *Atmos. Chem. Phys.*, **11**, 627–654.

Wood, R., et al., 2014: Cloads, Aaerosol, and Precipitation, in the Marine Boundary Layer: An ARM Mobile Facility Deployment. *Bull. Amer. Meteor. Soc.*

Yarnal, B. and J. D. Draves, 1993: A synoptic climatology of stream flow and acidity. *Clim. Res.*, **2**, 193–202.